To the Graduate Council:

I am submitting herewith a thesis written by Stanley Z. Peplinski entitled "Turbulence Effects on a Holographic Imaging System." I recommend that it be accepted in partial fulfillment of the requirements for the degree of Master of Science, with a major in Physics.

Ronald A. Belz, Major Professor

We have read this thesis
and recommend its acceptance:

Accepted for the Council:

Vice Chancellor
Graduate Studies and Research

TURBULENCE EFFECTS ON A HOLOGRAPHIC IMAGING SYSTEM

A Thesis

Presented for the

Master of Science

Degree

The University of Tennessee, Knoxville

Stanley Z. Peplinski

June 1978

1358035

ACKNOWLEDGMENTS

The author wishes to express his sincerest appreciation to his parents, Mr. and Mrs. Vincent Peplinski, for their love, sacrifice and support of this endeavor.

Special thanks are given to the author's advisor, Dr. R. A. Belz, for defining the topic for research and supervising the progress of the work. Thanks are also extended to Drs. R. H. Kohl and A. A. Mason for serving as members of the thesis committee. Appreciation is expressed to Mr. A. E. Lennert, Branch Manager of Advanced Concepts, ARO, Inc., for his support of the study. The author would also like to thank the many other people of ARO, Inc., who assisted in numerous ways to this effort.

The work reported herein was supported by Headquarters, Arnold Engineering Development Center (AEDC), Arnold Air Force Station, Tennessee, within the terms of Contract F40600-77-C-0003 with ARO, Inc. Reproduction to satisfy the needs of the U. S. Government is authorized.

ABSTRACT

A side-band holographic system used to record particle images in a high enthalpy environment is described. Holographic particle velocity and size data recorded through turbulent air conditions are presented along with the observed turbulence effects on the holographic image quality. The turbulence effects, background mottling, and loss of image resolution are shown to be functions of phase changes along planar and spherical wavefronts and are discussed in terms of the phase structure function and intensity variance. Holographic quality was found to be strongly dependent on the air stream pressure within the Aerodynamic and Propulsion Test Unit (APTU) wind tunnel. Suggestions for measuring the strength of air turbulence within the air stream in terms of the refractive index structure constant are made. Methods for reducing the turbulence effects on the holographic system are also presented.

LIST OF FIGURES

FIGURE		PAGE
1- 1.	Side-Band Hologram Recording and Reconstruction Geometry	3
2- 1.	Aerodynamic and Propulsion Test Unit Facility Schematic	12
2- 2.	Aerodynamic and Propulsion Test Unit Facility Arrangement	12
2- 3.	Nozzle Inlet Turbulence Level	14
2- 4.	Mixer Total Pressure Profile	16
2- 5.	Aerodynamic and Propulsion Test Unit Particle Monitor Laser Transmitter Optical System	17
2- 6.	Aerodynamic and Propulsion Test Unit Side-Band Holocamera Particle Monitor Optical System	19
2- 7.	Resolution of the Side-Band System	21
2- 8.	Side-Band Reconstruction Schematic	24
2- 9.	Histogram of Aerodynamic and Propulsion Test Unit Particle Size Data: Definite Images	26
2-10.	Histogram of Aerodynamic and Propulsion Test Unit Particle Size Data: Possible Images	26
2-11.	Photographs of Definite Pairs of Images: Double-Pulsed Hologram	27
2-12.	Average Blotch Size as a Function of Pressure	29
2-13.	Mottling of Background as a Function of Turbulence	30

FIGURE PAGE

2-14. Minimal Resolvable Diameters as a Function of Air Density: Near Port Window 31

2-15. Turbulence Effects on Far Reticle Edge 33

3- 1. Modulation Transfer Function (MTF) of Total Optical System [31]. 40

3- 2. Normalized Resolution for Short Exposure [26]. 42

3- 3. Turbulence Effect on Intensity Distribution. 46

4- 1. Hologram Quality as a Function of Phase Change 51

CHAPTER I

INTRODUCTION

Problem Statement

The work presented is an analysis of data recorded during an application of holographic particle sizing technology at Arnold Engineering Development Center (AEDC), Arnold Air Force Station, Tennessee. As such, the experimental results presented herein are based on a specific problem in holography; namely, degradation of holographic quality as a result of imaging through a turbulent medium. The theoretical discussion, however, is of a more general nature--that of propagating a laser beam through a randomly varying medium, i.e., the atmosphere. The coupling factor between experiment and theory is that air turbulence in a wind tunnel mixing chamber and in the atmosphere produces local fluctuations in the refractive index of the medium along the beam propagation path. The refractive index fluctuations cause amplitude and phase changes along the wavefront of the propagating beam which manifest themselves as a mottling of the background and reductions in image contrast, edge sharpness, and resolution.

Holography as a Research Tool

In 1948, Dennis Gabor [1][1] proposed a novel two-stage, lensless imaging process which he called wavefront reconstruction. This process,

---

[1]Numbers in brackets refer to similarly numbered references in the Bibliography.

known as in-line holography, received only mild interest in the early days. However, with the advent of the laser and changes in the original concept, many versions of the holographic techniques have been developed. Two good references describing these techniques are Goodman [1] and Smith [2]. The facility with which holography allows particle size distribution, velocity and density to be measured without physically interfering with the particle field has made this a useful tool for research and industry. Some successful applications of particle field holography have been to determine the liquid water content within an icing test facility [3], the visualization of combustion [4, 5], and the interaction of reacting sprays [6].

In addition to Gabor's in-line holography there is the side-band holographic technique, developed by Leith and Upatnieks. Since the experimental setup described in Chapter II is a side-band imaging system, the theoretical presentation of the recording and reconstruction processes of a hologram will be limited to this method.

Physics of Holography

Holography is a two-step process: recording an optical wavefront and its reconstruction. The basic physics involved in the formation of a hologram is that the film interferometrically records the amplitude and phase variations of the radiation associated with an image of the object. This information is so recorded that subsequent illumination of the hologram serves to reconstruct the original object wave.

Figure 1-1a shows the formation of a side-band (also called an off-axis) hologram. A single beam, originating from the laser source

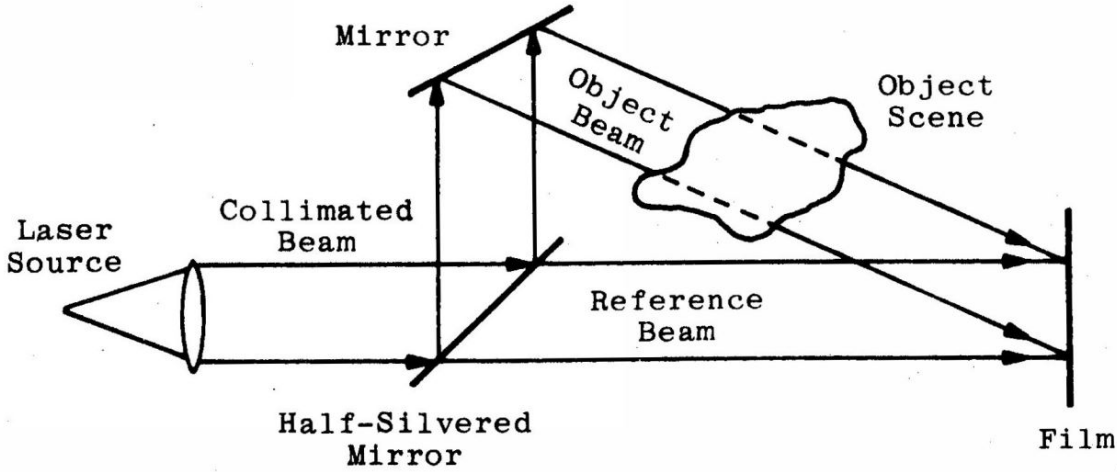

a) Recording of a side-band hologram

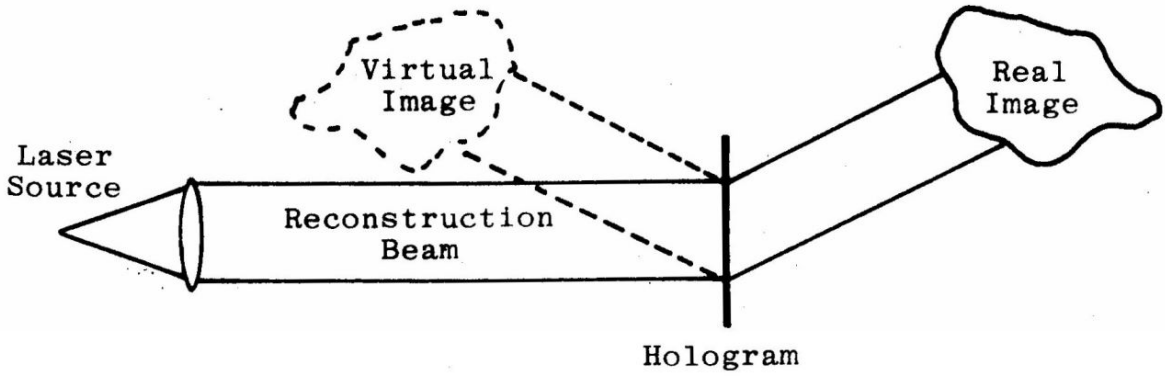

b) Reconstruction of a side-band hologram

Figure 1-1. Side-band hologram recording and reconstruction geometry.

is used to record the hologram. This beam is split into two components, one which is directed towards the object and the other towards the recording medium, a photographic film. The component that illuminates the object is partially scattered by the object. This scattered wave, called the object wave, then becomes incident upon the photographic film. At the same time another (reference) wave proceeds directly to the tilm, illuminating it at an angle ϕ, to produce characteristic interference fringes.

Mathematically the two waves can be expressed in terms of the amplitude (A), the phase (θ), and the angular frequency (ω) of the radiation being used. The object and reference waves, denoted by the subscripts o and r, respectively, are

$$E_o = A_o e^{i(\omega_o t + \theta_o)} , \tag{1-1a}$$

$$E_r = A_r e^{e(\omega_r t + \theta_r)} . \tag{1-1b}$$

Since both waves originated from the same source, $\omega_o = \omega_r = \omega$.

The total field at the recording plane is the sum of the two waves, i.e.,

$$U = E_o + E_r . \tag{1-2}$$

Since the recording medium is photographic film which responds only to intensity, then, by the Poynting theorem, the observed intensity is the product of the radiating field times its complex conjugate, i.e.,

$$I = UU^* . \tag{1-3}$$

Equation (1-3) then becomes

$$I = I_o + I_r + A_o A_r^* e^{i(\theta_o - \theta_r)} + A_o^* A_r e^{-i(\theta_o - \theta_r)} . \qquad (1\text{-}4)$$

The above equation may be interpreted physically as follows: terms one and two depend only on the intensities of the two beams, these bias the total film illumination. Terms three and four contain information which produce the virtual and real images of the objects in the reconstruction. Equation (1-4) can be simplified by using the cosine relationship to

$$I = I_o + I_r + 2\sqrt{I_o I_r}\cos(\theta_o - \theta_r) . \qquad (1\text{-}5)$$

In the holographic process the phase term contains the information about the object. Since the phase is more important than either of the wave amplitudes, an analysis of phase changes due to the medium of propagation will be made in the latter part of this chapter.

Once the amplitude and phase information about the object has been recorded it remains to develop the photographic film and reconstruct the optical field of the object. Figure 1-1b depicts the reconstruction process of the side-band hologram. When the developed film is illuminated by a coherent source, at the same angle as the reference beam was in the recording, the real and virtual images of the object are reconstructed. They are located on either side of the hologram and are at the same angle that the object beam impinged onto the film. If plane waves of the same wavelength are used throughout the entire process, the images are reconstructed exactly in size and position as the original object was relative to the film.

Phase Mismatch

Having discussed the basic physics of the recording and reconstruction of side-band holograms, an analysis of the phase mismatch between the object wave propagating in a turbulent and nonturbulent medium will be made. Since both waves pass through different media before striking the photographic film, the phase of each wave will then be dependent on the refractive index, n, of the medium that the wave passes through. The phase of both waves can be expressed as

$$\theta_o = kn_oL \ , \tag{1-6a}$$

$$\theta_r = kn_rL \ , \tag{1-6b}$$

where k is the free-space wavenumber ($k = \frac{2\pi}{\lambda}$) of the radiation, and L is the propagation length. The propagation length is assumed to be the same for both waves. Assuming only a small difference between the indices of refraction of the two media, one can write

$$n_o \approx n_r + \Delta n \ . \tag{1-7}$$

The phase difference ($\Delta\theta$) then becomes

$$\Delta\theta \triangleq \theta_o - \theta_r \approx kL\Delta n \ . \tag{1-8}$$

The Dale-Gladstone [7] equation relates the refractive index to the density of that medium by

$$n - 1 = k'\rho \ , \tag{1-9}$$

where k' is the Dale-Gladstone constant, and ρ is the density of the medium. Therefore, a change in density ($\Delta\rho$) yields a corresponding change in the refractive index by the amount

$$\Delta n = k'\Delta\rho \ , \tag{1-10}$$

and Eq. (1-8) becomes

$$\Delta\theta \approx kLk'\Delta\rho \ . \tag{1-11}$$

The Ideal Gas Law [8] relates the density of the medium to the pressure (P) and the temperature (T) by

$$P = R\rho T \ , \tag{1-12}$$

where R is the gas constant. Using the Ideal Gas Law to relate changes in density to changes in pressure and temperature then gives

$$\Delta\rho = \rho\left(\frac{\Delta P}{P} - \frac{\Delta T}{T}\right) \ . \tag{1-13}$$

From the above relation, Eq. (1-11) becomes

$$\Delta\theta \approx kL(n-1)\left(\frac{\Delta P}{P} - \frac{\Delta T}{T}\right) \ . \tag{1-14}$$

Equation (1-14) shows that the propagation of the object wave in two different media shifts the phase of the wave by an amount $\Delta\theta$; the degree of phase change being proportional to the strength of the density fluctuations (Eq. (1-13)) which are measured by pressure and temperature variations.

Since a hologram records the phase information of a wave, any distortion of the object wave, due to the medium of propagation, will alter the information reaching the photographic film. In the reconstruction process this distorted wavefront will be reproduced and will manifest itself as a mottling of the image background, loss of image resolution, or a spreading of the image. The net result is a loss of holographic quality.

In Chapter II the experimental optical systems for recording and reconstructing side-band holograms are presented. The wind tunnel facility and its turbulent airflow, through which the object beam of the side-band holocamera passed, are also discussed. The experimental resolution of the holographic system is compared to theory. An analysis of turbulence effects on background mottling and loss of image resolution, in terms of the air pressure and density, is presented. The theoretical effects of air turbulence on propagating laser beams are discussed in Chapter III in terms of atmospherically observed effects. Statistical expressions for fluctuating parameter, such as the refractive index of the medium and the phase and intensity of the beam traversing the medium, will be developed. In Chapter IV the theoretical expressions obtained in Chapter III will be discussed in terms of the refractive index structure constant of the turbulent airflow within a wind tunnel. These expressions, along with known turbulence, will be used to predict, to a first approximation, the quality of the holograms that would be recorded under such conditions. Suggestions

for further investigation along these lines are also made. Alternatives for recording holographic images through turbulent media are presented in Chapter V, along with turbulence effects on automated reconstruction systems.

CHAPTER II

EXPERIMENTAL SETUP

Introduction

The primary purpose of the holographic particle monitoring system at AEDC's Aerodynamic and Propulsion Test Unit (APTU) was to determine the particle size distribution, concentration, and velocity, with a secondary purpose of determining the effects of the turbulent air stream on coherent images. Because of the simplicity of the optical system, an in-line holocamera was initially set up. However, the passage of the reference beam and the object beams through the test cell, where the level of air turbulence was very high, reduced the spatial coherence of the light reaching the film, causing a significant loss of image resolution. Because of the turbulence problems encountered with the in-line configuration a side-band optical system was set up. Since the reference beam is routed around the test cell before reaching the film, image resolution should not suffer as much from the air stream turbulence. It so happened that at the same time the side-band system was being installed, alterations within the test cell were also being made to increase air mixing and to eliminate a strong central hot air core. These changes decreased the level of pressure fluctuation from 3.5 to 0.7%. Under these improved wind tunnel conditions side-band holograms were taken and particle size data were obtained. No comparison could be made between in-line and

CHAPTER II

EXPERIMENTAL SETUP

Introduction

The primary purpose of the holographic particle monitoring system at AEDC's Aerodynamic and Propulsion Test Unit (APTU) was to determine the particle size distribution, concentration, and velocity, with a secondary purpose of determining the effects of the turbulent air stream on coherent images. Because of the simplicity of the optical system, an in-line holocamera was initially set up. However, the passage of the reference beam and the object beams through the test cell, where the level of air turbulence was very high, reduced the spatial coherence of the light reaching the film, causing a significant loss of image resolution. Because of the turbulence problems encountered with the in-line configuration a side-band optical system was set up. Since the reference beam is routed around the test cell before reaching the film, image resolution should not suffer as much from the air stream turbulence. It so happened that at the same time the side-band system was being installed, alterations within the test cell were also being made to increase air mixing and to eliminate a strong central hot air core. These changes decreased the level of pressure fluctuation from 3.5 to 0.7%. Under these improved wind tunnel conditions side-band holograms were taken and particle size data were obtained. No comparison could be made between in-line and

side-band holograms since they were taken under different test cell configurations.

In this chapter the APTU facility, its air turbulence, the holographic systems used within the facility, and the holograms taken at various combinations of pressures and temperatures will be presented and discussed.

Test Site

The APTU wind tunnel, illustrated schematically in Fig. 2-1, is a high enthalpy facility designed primarily for free-jet development of supersonic/hypersonic propulsion systems. Generation of the high enthalpy airflow employs a high pressure/temperature mixing process. Stagnation conditions of the free-jet nozzle are established in the forward adapter section (Fig. 2-2), a 7-foot diameter plenum chamber located immediately downstream of the air mixer, by a controlled blending of high temperature (primary) air from a pebble bed heater with cold (secondary) air from the storage reservoir. Control of the air parameters is managed by a computer system using averaged data derived from a control rake located in the free-jet nozzle plenum. The plenum between the control rake and the free-jet inlet (Fig. 2-2) was the region of investigation by the holographic system.

Aerodynamic and Propulsion Test Unit Airflow Dynamics

An analysis [9] of the APTU air mixing process indicated that the parameter most likely to have a strong effect on the level of turbulence in the air stream was the momentum ratio, R_m, defined as

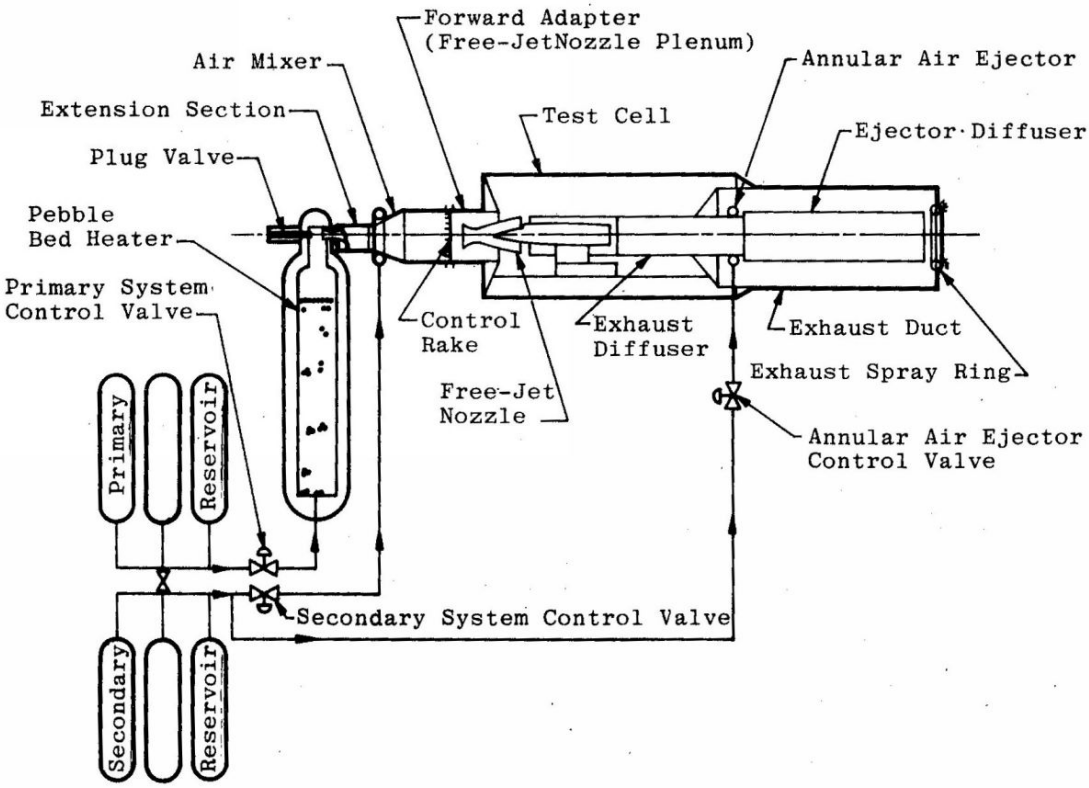

Figure 2-1. Aerodynamic and Propulsion Test Unit facility schematic.

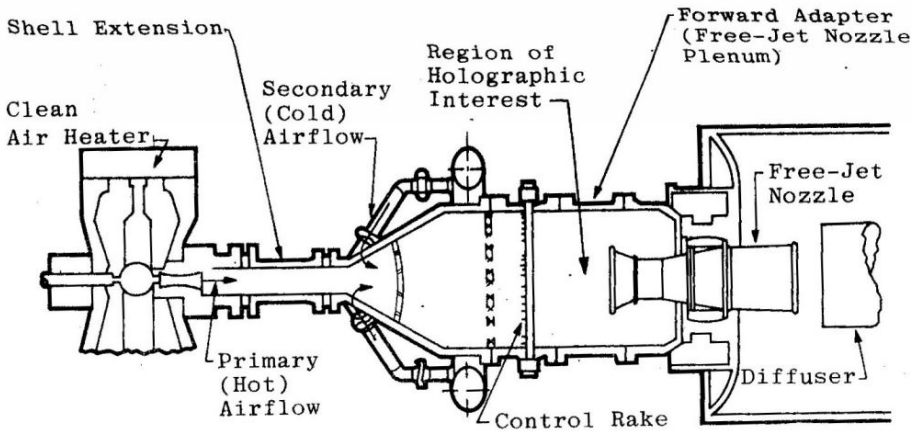

Figure 2-2. Aerodynamic and Propulsion Test Unit facility arrangement.

$$R_m = \frac{\dot{m}V_2}{\dot{m}V_1} \; \frac{\text{secondary}}{\text{primary}} \quad , \tag{2-1}$$

R_m is a dimensionless ratio of secondary to primary flow momentum computed in the plane of initial mixing. The test conditions were selected to provide a range of R_m from 0.2 to 8 while simulating, within the free-jet plenum, stagnation conditions of pressure and temperature typical of expected user conditions. Momentum ratio was varied by changing the stagnation conditions and by varying the temperature of the primary flow for a given stagnation condition. Pressure and temperature measurements were taken by high frequency response instruments mounted on the control rake to monitor test cell conditions.

Aerodynamic and Propulsion Test Unit airflow dynamics were caused by a strong shock in the shell extension section (Fig. 2-2) initiated by the expansion of the primary flow from the high pressure environment of the pebble bed heater and by a strong high pressure core along the mixer centerline. To elliminate the central core a core-breaker (Fig. 2-2), an elliptical dish drilled to lower porosity in the center region, was installed to diffuse the airflow more uniformly across the mixer cross section. A low porosity screen (6 x 6 mesh) and screen support were designed to further dampen flow dynamics and reduce the scale of turbulence. With the installation of these two systems flow distortion was significantly reduced.

The level of turbulence, defined as the ratio of ΔP_{RMS} to the total pressure, P_T, is shown in Fig. 2-3 for a series of tests. For the range of momentum 0.6 to 2, the turbulence is approximately 0.7%. The flow field in the mixer was also examined to determine the total

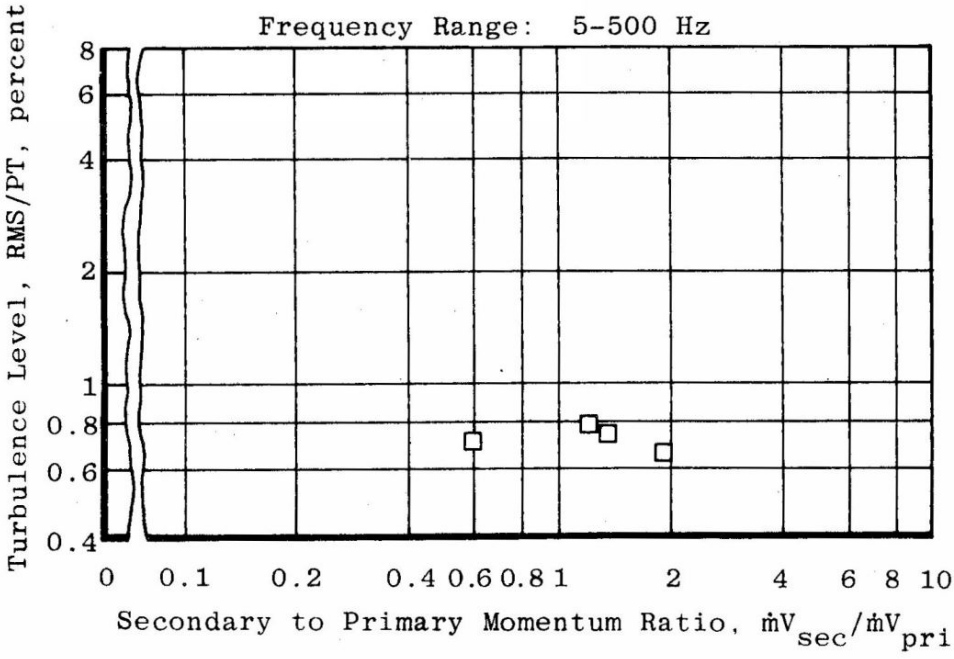

Figure 2-3. Nozzle inlet turbulence level.

pressure profile. The total pressure distortion was found to be almost uniform across the radius of the mixer. Figure 2-4 demonstrates this for a momentum ratio of 0.9.

Side-Band Holographic Arrangement

The side-band holocamera consisted of a transmitting optical system (a ruby laser, laser alignment and collimating optics) on one side of the air mixer and a telescopic receiving optical system on the other side. The laser transmitting optics system, Fig. 2-5, was mounted on a temperature controlled, water cooled aluminum base plate to minimize changes in the laser cavity length due to ambient temperature changes in the APTU environment; thereby assuring consistent firing of the ruby laser. A 5 mw helium-neon (He-Ne) laser was used to align the holocamera optical system. An auto-collimator was used to align the ruby laser cavity. The Q-switched ruby laser is capable of transmitting 30 millijoules per pulse in the dominant TEM_{00} mode. Mode selection is accomplished by a smaller intra-cavity aperture and an etalon for the transverse and longitudinal modes, respectively. A beam expanding telescope collimated the laser beam to a 2-inch diameter.

Because of the high levels of mechanical vibrations and acoustical noise expected in the APTU cell environment during tests, precautions were taken to minimize the chances of damage either to the laser or to the transmitting optical system. The transmitting optical system was enclosed in a metal box, covered with a 2-inch thick sandwich of rubber foam and lead plate, for acoustical isolation, and placed on pneumatic isolators to reduce mechanical vibrations.

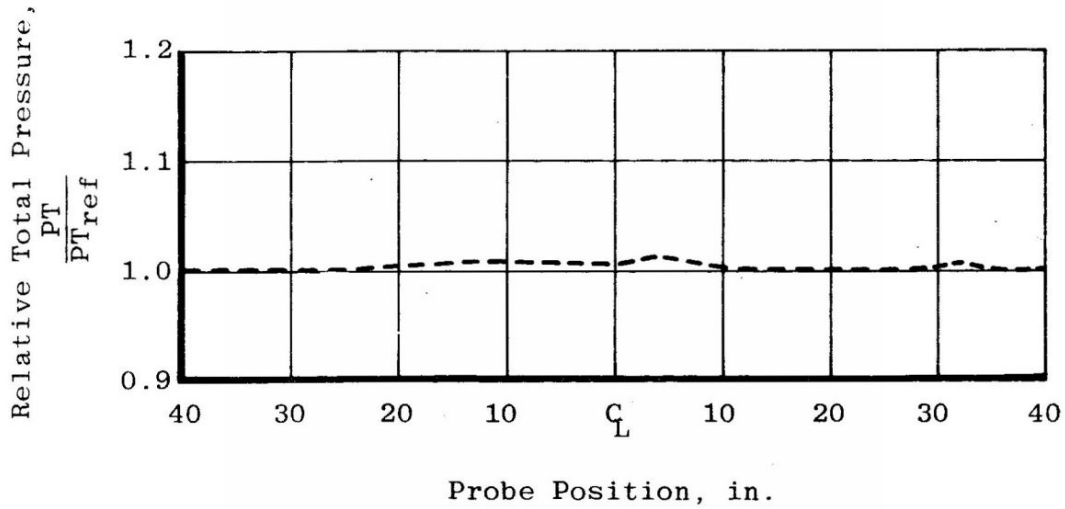

Figure 2-4. Mixer total pressure profile.

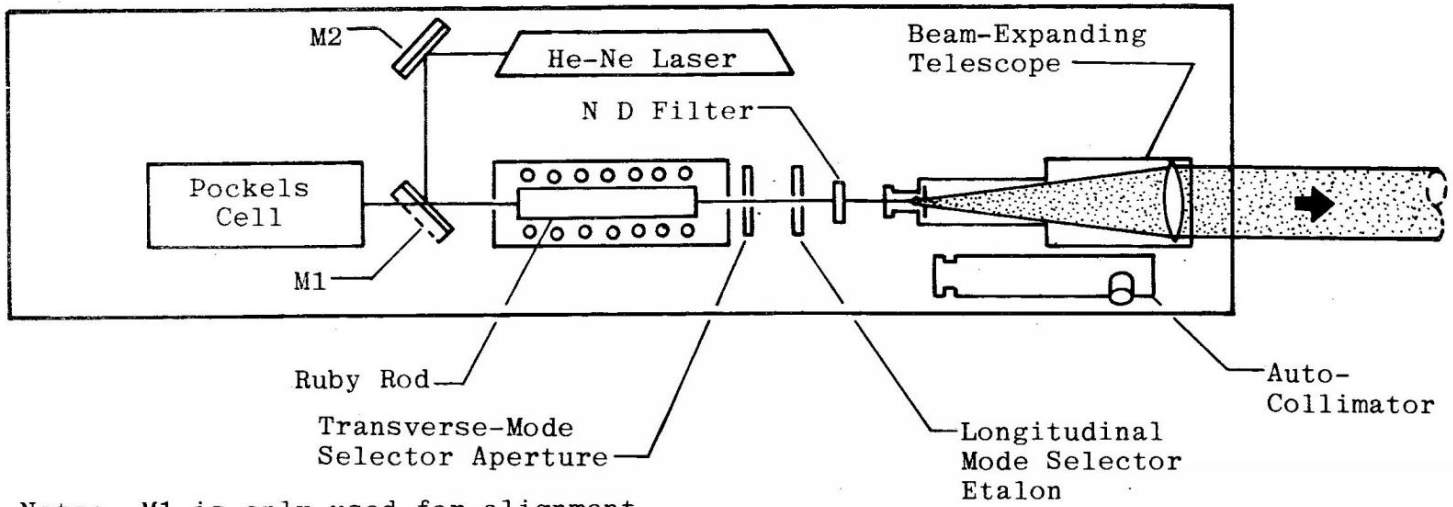

Note: M1 is only used for alignment purposes and is removable.

Figure 2-5. Aerodynamic and Propulsion Test Unit particle monitor laser transmitter optical system.

The optics of the side-band holography system (shown in Fig. 2-6) consists of a 50% beam splitter to create the object and reference beams and mirrors which direct the beam to the film. A pair of imaging lenses in the object beam focus the film plane onto the centerline of the test cell and demagnify the object field; causing a reduction in the object size by 0.62 and compressing the 3.5-foot radius of the mixer volume to a more manageable length of 26 inches on the reconstruction bench.

The resolution of the side-band holocamera imaging optical system depends on two factors:

1. The limiting resolution (R) in the recording due to a limiting aperture of the imaging optics, which is expressed as

$$R = \frac{2.44\ \lambda Z_0}{D}\ , \tag{2-2}$$

   where D is the limiting aperture and Z_0 is the lens-to-object distance. For particles within 8 inches of the centerline of the mixer the limiting aperture was the 2-inch port window. However, for those close to the near window, the second (and smaller) of the two imaging lenses determined the limiting aperture.

2. The resolution is also determined by the object distance, Z_1, from the film plane. For an optical system preceding the film plane, Z_1 is the distance between the film and the final image formed by the lenses. Thompson [10] suggests

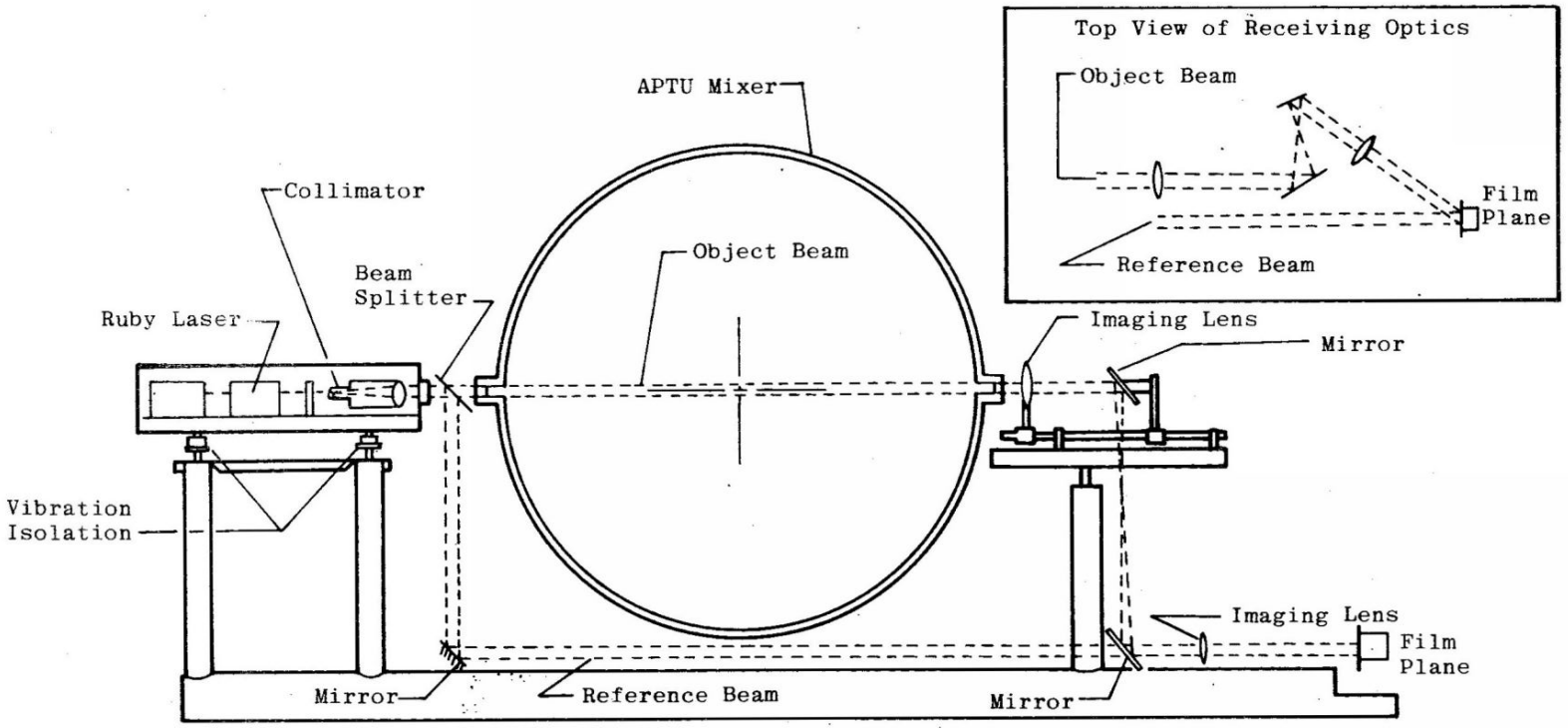

Figure 2-6. Aerodynamic and Propulsion Test Unit side-band holocamera particle monitor optical system.

that the film-to-object distance not exceed 100 far-fields. Therefore,

$$Z_1 \leq 100 \frac{d^2}{\lambda} , \tag{2-3}$$

where d is the object diameter.

It can easily be shown that the resolution of the reconstructed particle images will not be affected by the demagnification. The optical system forms a demagnified image of the object of dimension

$$d' = md , \tag{2-4}$$

where m is the demagnification. From the thin lens equation, $m^2 Z_1$ is the incremental distance increase, Z_1', of the image from the film plane, with respect to an incremental increase of the object distance. Substituting into Eq. (2-3) yields an identical expression for the image distance and size, i.e.,

$$Z_1' \leq 100 \frac{d'^2}{\lambda} . \tag{2-5}$$

The optical system imaged the centerline of the air mixer near the film plane. In the reconstruction the image plane focused 38 inches from the near port window. With this, the limits of the resolution of the side-band holograms imposed by the optical system and hologram recording are illustrated in Fig. 2-7. Near the port windows the hologram recording limits the resolution to 80 μm and 95 μm at the near and far port windows, respectively. The resolution

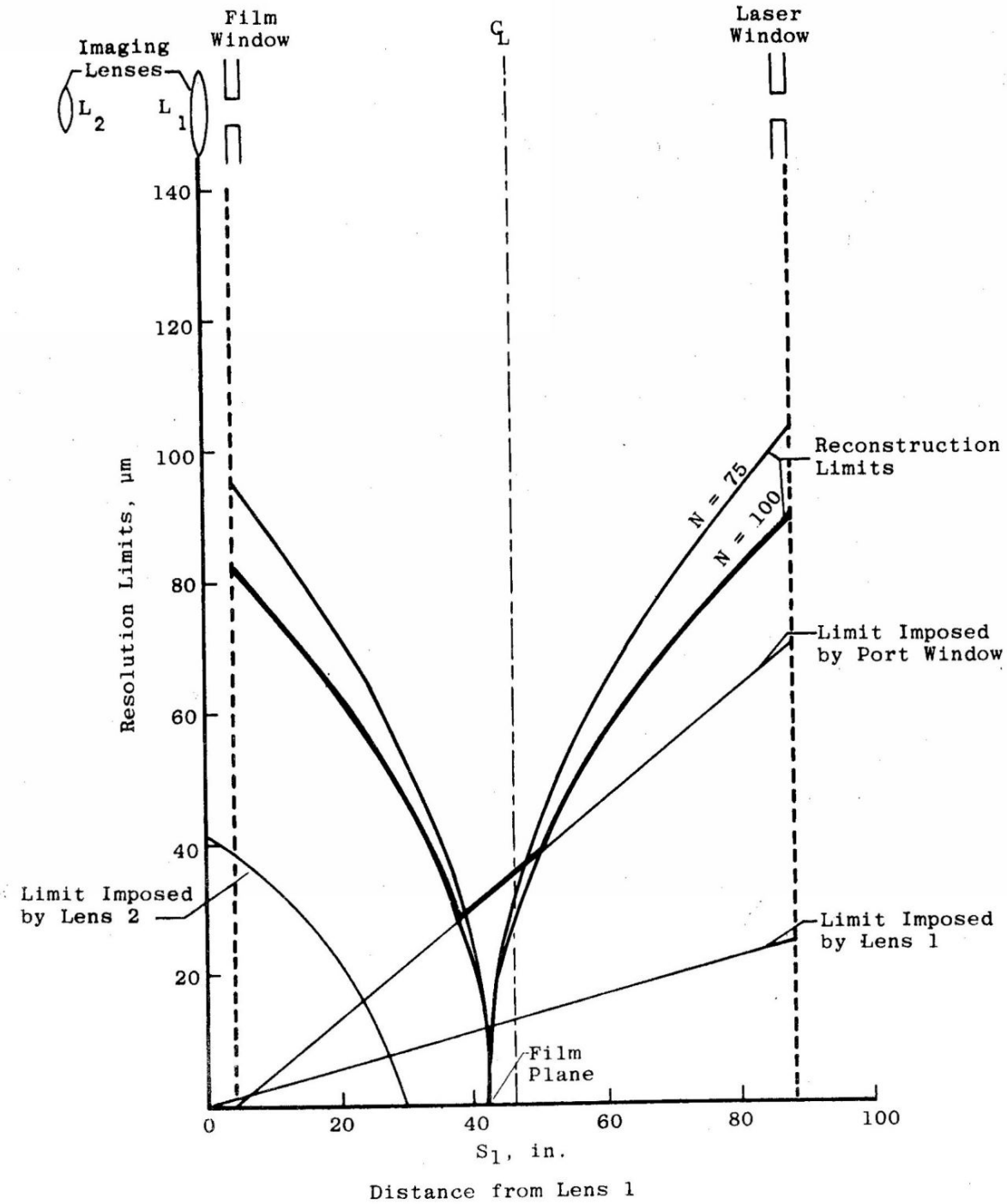

Figure 2-7. Resolution of the side-band system.

near the film plane is determined by the size of the port window to be 30 μm; no matter how good the imaging optics are.

Holographic Test Data

The region where holograms were recorded was between the control rake and the free-jet nozzle inlet and is shown in Fig. 2-2, page 12. It was believed that particles, loosened from the pebble bed heater and entrained in the air stream, were entering the model test cell volume. Holographic data were to provide size distribution and velocity of the particulates within the air stream. To accommodate the passage of the laser beam through the APTU mixer, quartz windows were placed on both ports of the air mixer. Patterson reticles were placed on each port window to determine the degree of resolution loss under operating conditions.

Holograms were recorded automatically by the APTU control computer. Once the power supply charged to a set voltage, the laser was fired after opening the shutter on the film magazine; the film advanced after the shutter closed. All the data were recorded on 4 x 5-inch glass plates which were identified by exposing a corner of the plate with a two-digit light emitting diode (LED) array. During a test run holograms were taken every 25 seconds, which was the charging rate of the laser power supply.

Holograms were taken at various stagnation conditions within the air mixer. The air stream temperature ranged from 527 to 1100°R while pressures varied by an order of magnitude (14 to 130 psia). This spread of air conditions allowed the holographic data to be analyzed to determine the effects of mixer air conditions on hologram quality. The

stagnation conditions were measured by high frequency transducers on the control rake. The pressure transducers inadvertently picked up the electro-magnetic discharge from the laser power supply as spikes on the pressure curves, thereby indicating the exact pressure and time that the holograms were taken.

Reconstruction

The developed holograms were reconstructed using a He-Ne laser and the images were examined with a closed-circuit television (CCTV) reconstruction system, shown schematically in Fig. 2-8. The collimated beam from the 15 mw laser illuminated the hologram at the original reference beam angle producing two, real and virtual, nonoverlapping images of the original scene separated in space by an angle $\pm\phi$, relative to the reference beam. For three-dimensional scanning of the reconstructed volume the CCTV system was mounted on a motor-driven traverse. Once an image was identified, the operator indicated its position on the CCTV monitor with a light pen, and a Millipore πMC image analysis system measured the selected image parameter (area, Feret's diameter, etc.). These data were recorded on punched tape and later processed by a computer.

From holograms taken under pretest conditions the near and far reticle images were reconstructed. On these reticles were calibration spots of known sizes, ranging from 10 to 450 μm. The smallest resolved images were 80 μm and 120 μm for the near and far reticles, respectively. This is in excellent agreement with the predicted values near the port windows of Fig. 2-7.

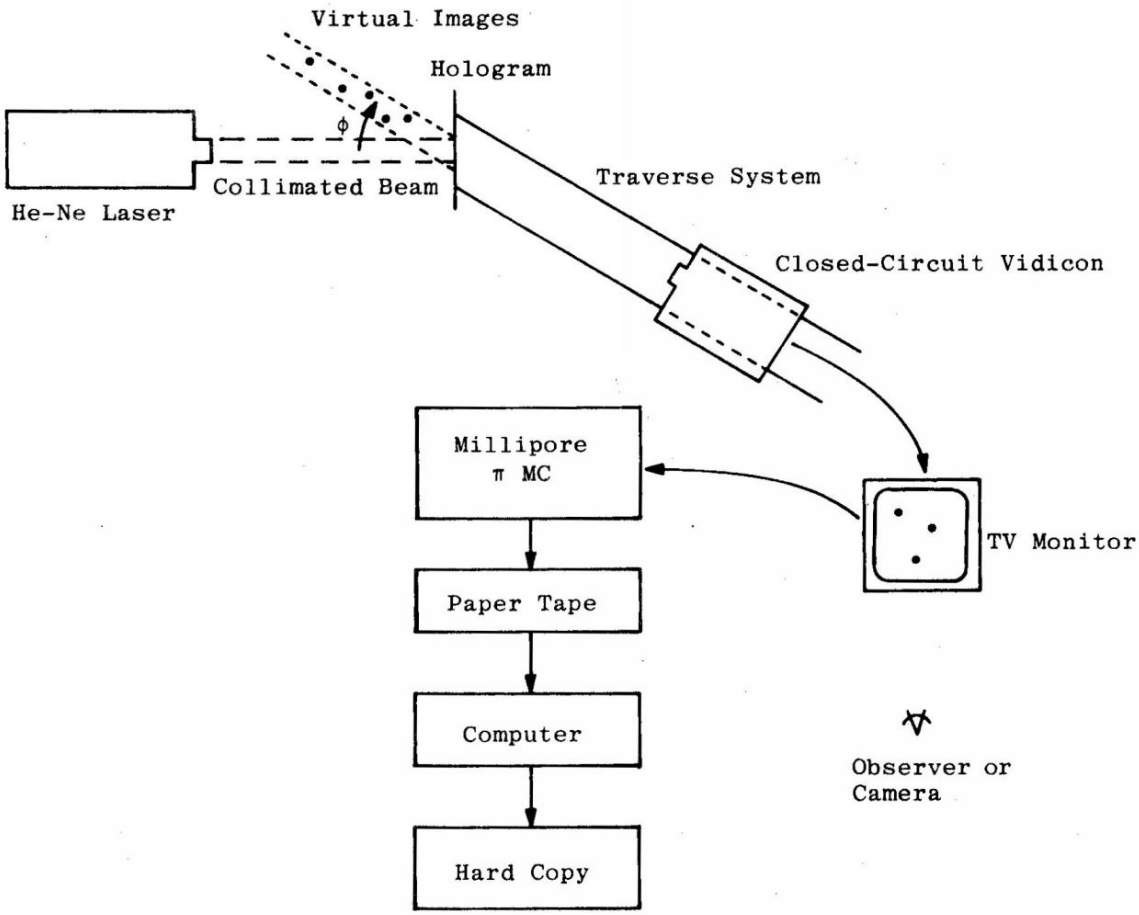

Figure 2-8. Side-band reconstruction schematic.

Histograms of the particle sizes found within the air stream are presented in Figs. 2-9 and 2-10. The cut-off of the data at 40 μm was due to the resolution limits imposed by turbulence in the air stream. The largest particle image found was 360 μm in diameter. The particle size data are plotted separately to distinguish images that came into focus with characteristic diffraction rings (Fig. 2-9) from those without rings (Fig. 2-10). The latter images were considered to be questionable since in many cases it was difficult to distinguish between particle images and background noise.

Double-pulsed (15 μsec pulse separation) holograms were also taken to determine the velocity of the particles within the flow. Data revealed velocities on the order of 7 to 20 meters per second. Photographs of image pairs for double-pulsed holograms are presented in Fig. 2-11. The photographs indicate the quality of the images and the degree of background mottling under different air stream conditions. Similar results were found for single-pulsed holograms taken at the same temperatures and pressures.

The ease of reconstructing particle images was found to be due to three factors: the sharpness of the image edge, the image contrast relative to the background, and the mottling of the background. Menzel [11] has shown that turbulent air acts as a low-pass filter reducing the sharpness of the image edge. It was noticed that as the pressure increased so did the mottling of the background. From a series of holograms taken at various combinations of pressure and temperature on two different test dates, the sizes of the background "blotches" were measured and the average values plotted with respect to pressure, temperature, and air density (which is proportional

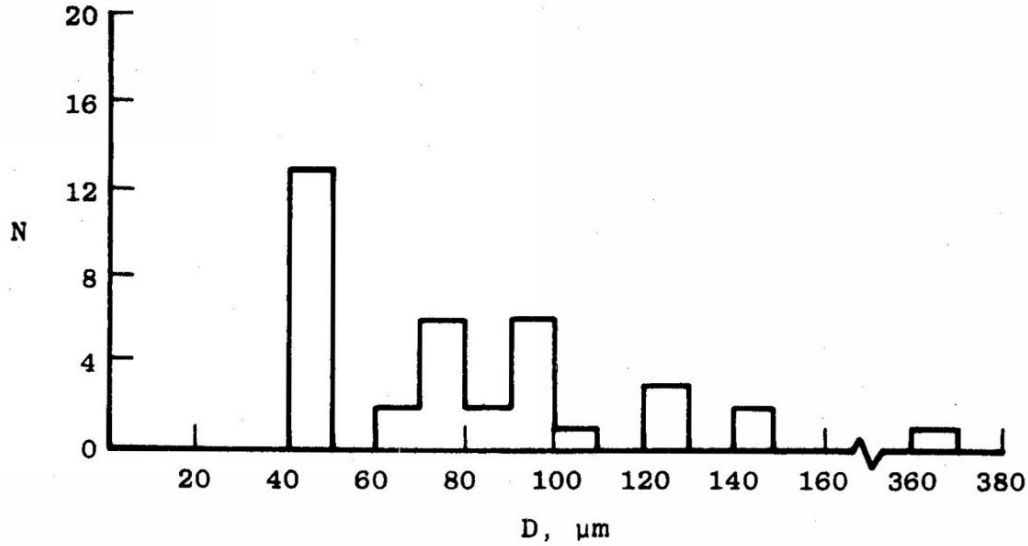

Figure 2-9. Histogram of Aerodynamic and Propulsion Test Unit particle size data: definite images.

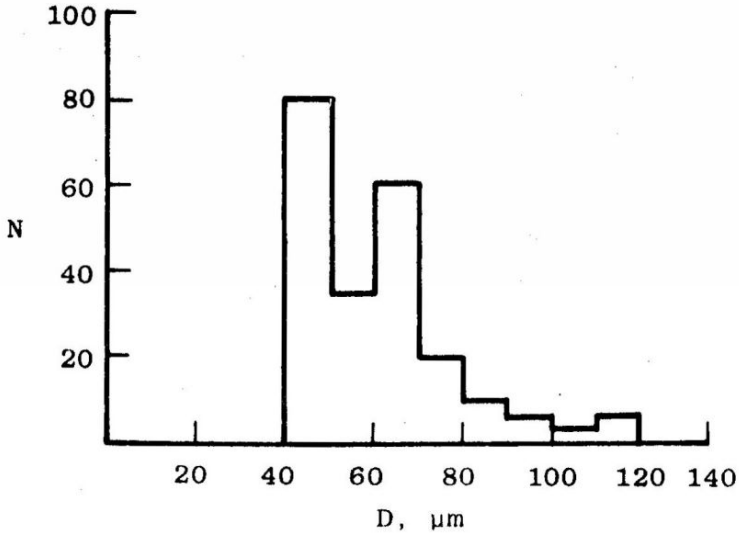

Figure 2-10. Histogram of Aerodynamic and Propulsion Test Unit particle size data: possible images.

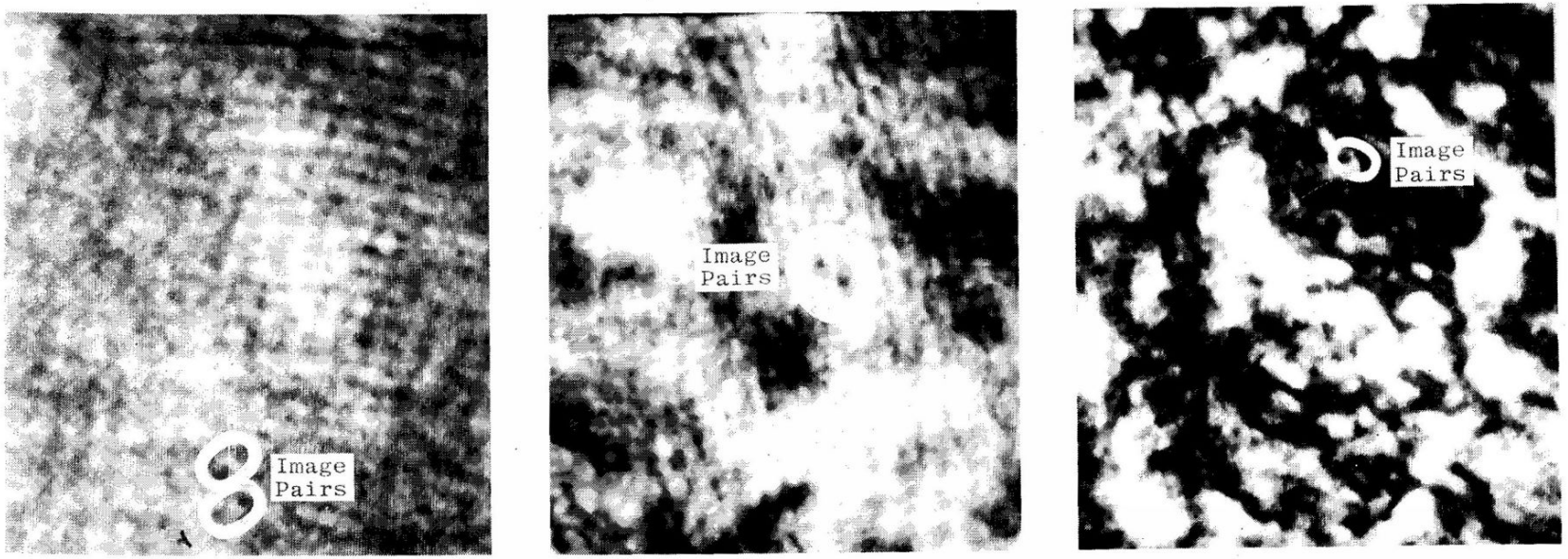

a) 20 psia/540°R b) 32 psia/1062°R c) 60 psia/890°R

Figure 2-11. Photographs of definite pairs of images: double-pulsed holograms.

to P/T). In Fig. 2-12 the correlation between pressure and the size of the mottling is shown. As the pressure increased the size of the blotches decreased with a corresponding decrease in image quality. The data from test date B are seen to be consistently lower than that from test date A. The analysis with density was not as conclusive. Likewise, no correlation could be found with temperature.

As the mottling increased it became more difficult to identify images. Particle images were difficult to discern from the blotches which were of similar size and intensity, thereby reducing the resolution capability of the holographic system. An analysis to show the effects of pressure, temperature, and density on the resolution of the holograms was made using two reticles mounted on the near and far port windows of the test cell. The reticles were reconstructed and the smallest calibration spot on the reticle was noted and data were plotted as a function of pressure, temperature, and P/T. Figure 2-13 demonstrates the turbulent background upon which these calibration images were superimposed. The best correlation of particle resolution in this case was made with density (i.e., P/T). The resolution limit for particles close to the near port window, plotted against density in Fig. 2-14, increased from 80 μm at pretest to 225 μm at P = 131 psia and T = 907°R for test date A. For test date B the resolution under similar conditions was worse by 160% (i.e., 360 μm). The loss of resolution on the second test date for the same ratio of P/T would indicate the presence of more turbulence on that day. On the second test date the number of cold air ducts, which generate the secondary airflow in the mixer, was reduced from eight to four. However, to keep

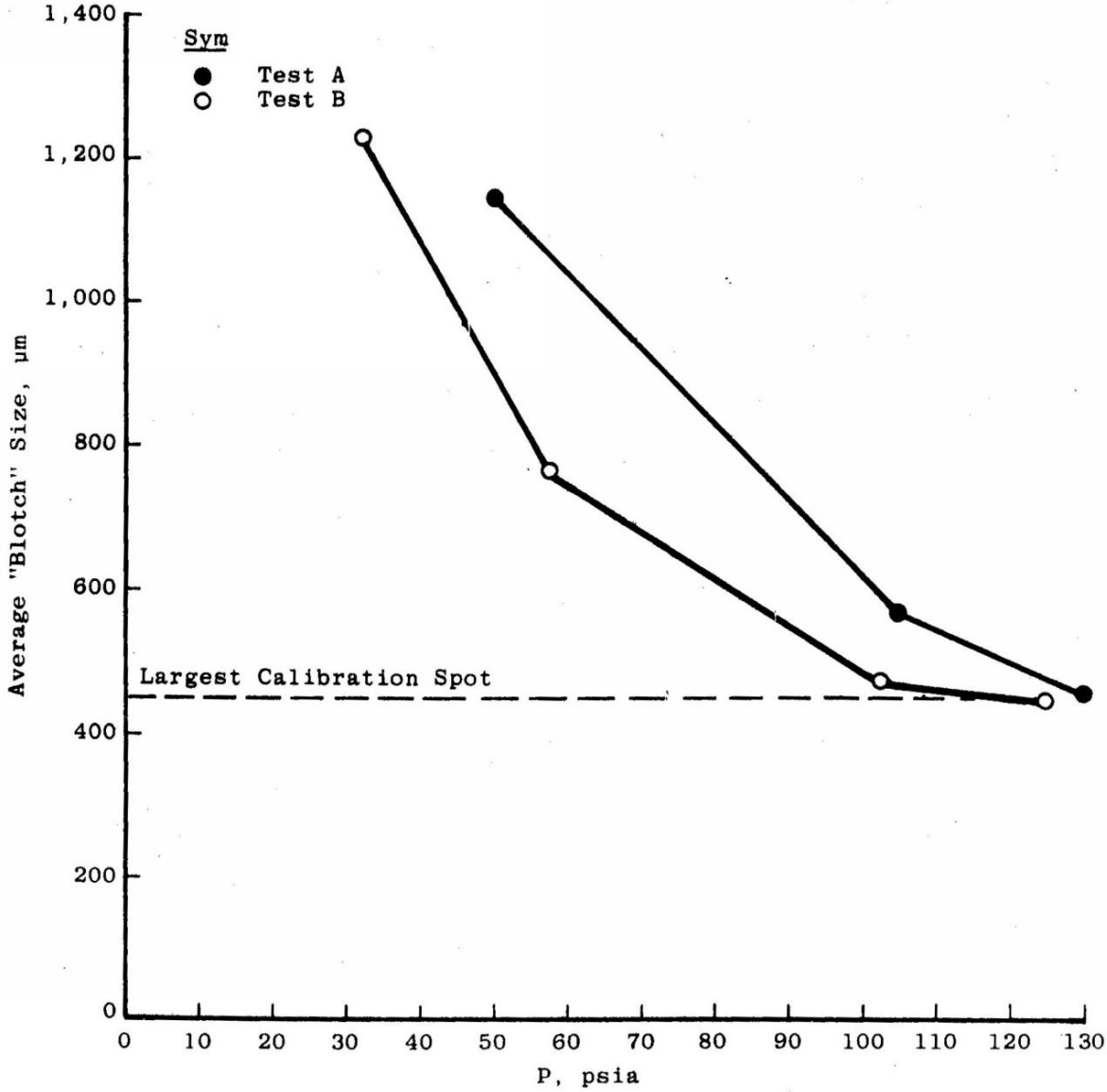

Figure 2-12. Average blotch size as a function of pressure.

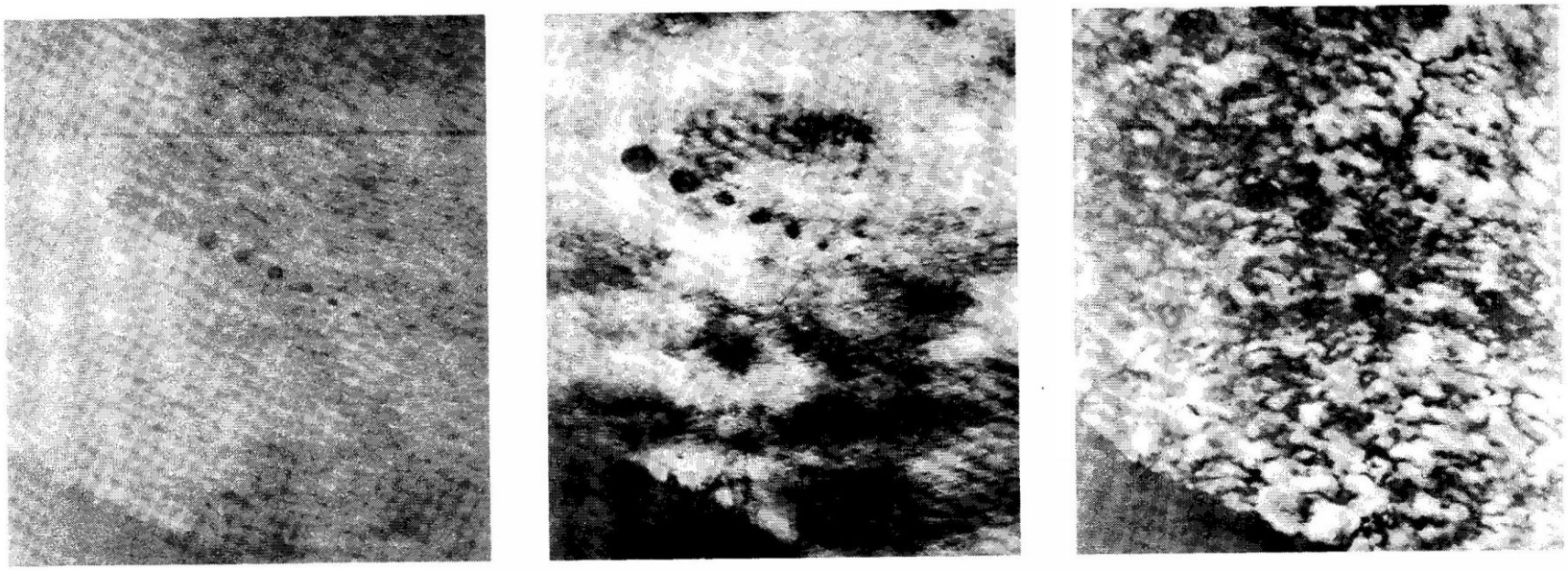

a) 20 psia/540°R b) 32 psia/1110°R c) 125 psia/1015°R

Figure 2-13. Mottling of background as a function of turbulence.

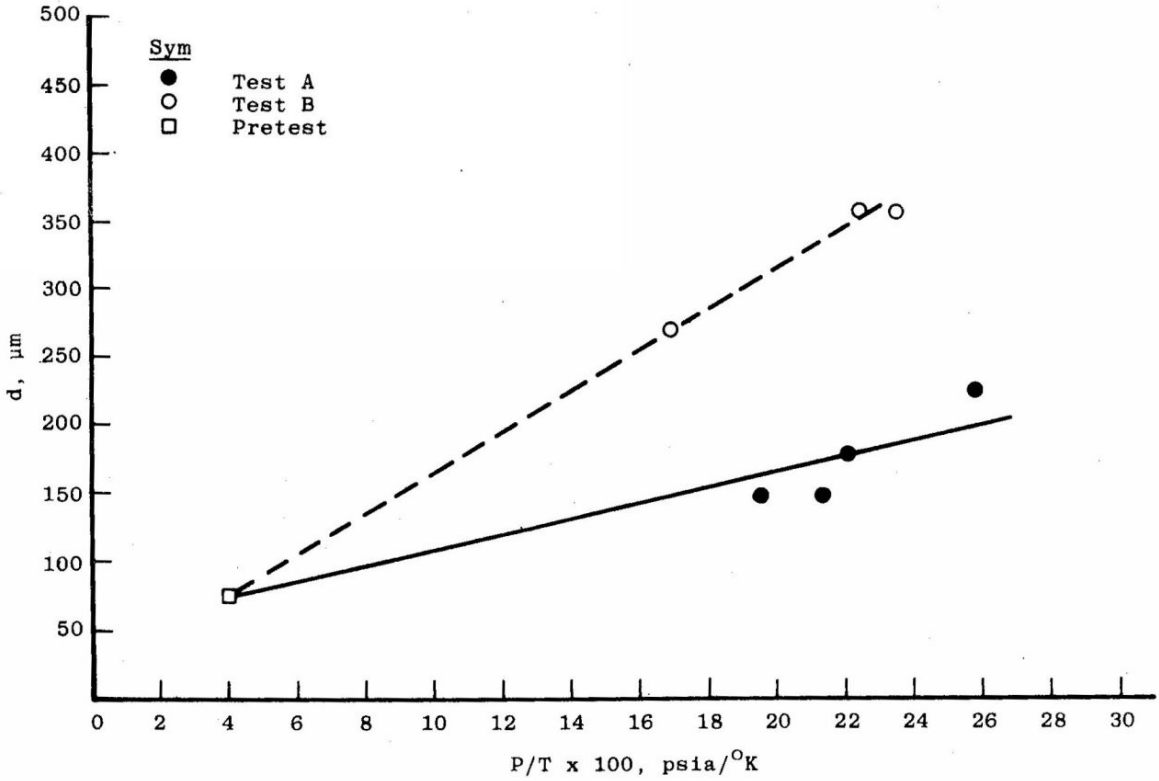

Figure 2-14. Minimal resolvable diameters as a function of air density: near port window.

the mass flow rate the same as before, the flow pressure was doubled; resulting in more air turbulence.

A similar analysis to determine the experimental resolution limit for the reticle on the far (laser) side of the air mixer, under flow conditions, was attempted. At pretest, with no airflow on, 120 μm resolution was achieved. But with airflow, the resolution dropped to 450 μm for the same temperature and pressure. It was impossible to make any further comparisons at higher mixing conditions since the largest spot on the reticle (450 μm) was not resolvable at these conditions. The edge of the far reticle was recognizable and is presented in Fig. 2-15 to illustrate the degradation.

Summary

Single- and double-pulsed holograms were taken through a high enthalpy environment. The range of stagnation conditions within the test cell was 14 to 130 psia and 507 to 1100°R. Particle size and velocity data were measured from holograms that were recorded at pressures of 60 psia or less. No holographic images could be reconstructed above 60 psia. Air pressure and density effects were correlated to background mottling and image resolution, respectively. No correlation, of any kind, was evident with temperature. This anomaly is explained by the fact that holograms were taken under conditions where the temperature was doubled; whereas, there was an order of magnitude increase in pressure.

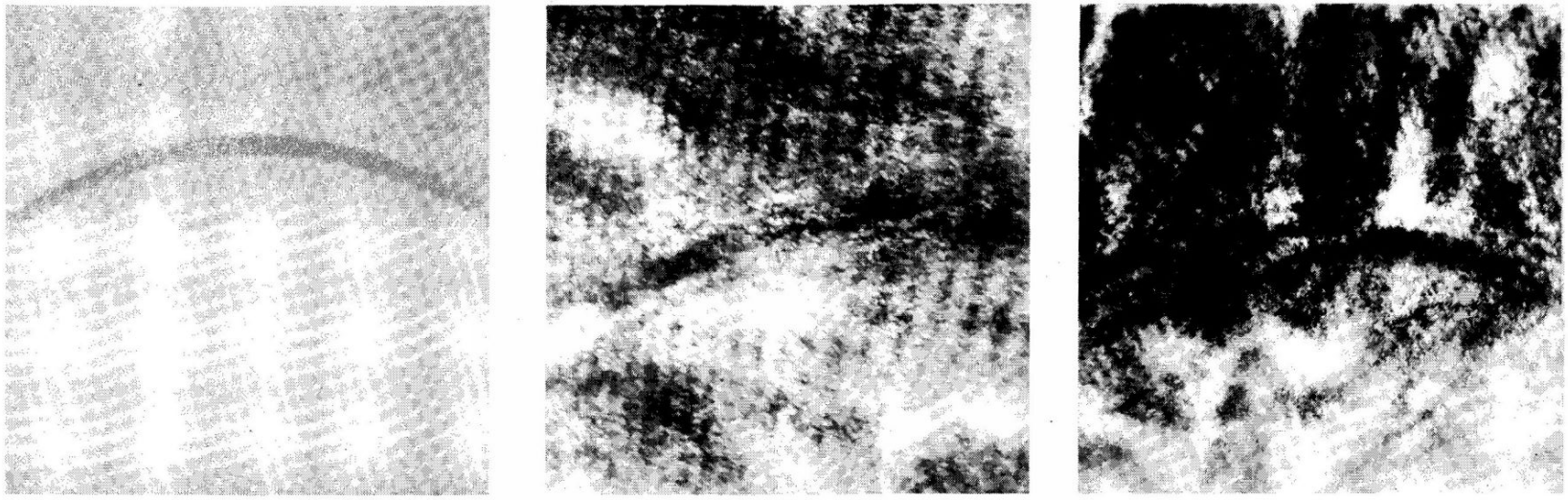

a) Pretest - no airflow b) 25 psia/887°R c) 50 psia/535°R

Figure 2-15. Turbulence effects on far reticle edge.

CHAPTER III

TURBULENCE EFFECTS ON THE PROPAGATION OF OPTICAL INFORMATION

Introduction

In analyzing the quality of a hologram several parameters must be considered: 1) film emulsion, 2) particle number density, and 3) medium of propagation. After viewing the side-band holograms taken at APTU, obtaining particle data and comparing these holograms to those taken under various number densities, it was concluded that the degradation of the quality of the APTU holograms was primarily due to the media. Since the air stream within the APTU mixer is turbulent and characterized by random parameters, a literature survey was conducted of turbulence effects on holographic recordings and laser beam propagation through randomly varying medium.

The survey revealed minimal research of turbulence effects on holographic processes. The only studies made were on Fourier-lensless holography [12, 13] through turbulent media, simulation of turbulence by shower glass [14, 15, 16], and milk-like solutions [17]. On the other hand, effects of atmospheric perturbations on planar and spherical waves have received considerably more attention, notably by Tatarski [18], Fried [19 through 26], and others [27 through 30]. Within this chapter the literature survey will be utilized to analyze turbulence (density gradients) effects on a holographic system.

An off-axis holographic system is like high-speed photography in the sense that the object is essentially frozen in time; since any

change in the scene has a characteristic time that is longer than the time it takes to make a photograph. Furthermore, the object beam of the side-band system (as in photography) must pass through the medium; whereas, the reference beam circumvents the medium. Therefore, in the reconstruction process the reference beam is identically reproduced; whereas, the original object beam is not, due to distortions encountered in passing through the medium. This analysis is then limited to the effects of the medium on the object beam.

Wave Statistics

In order to determine the effects of turbulence on a propagating laser beam the characteristics of the turbulence must be known such that an exact solution to the reduced scalar wave equation,

$$\nabla^2 E(x) + k^2 n(x) E(x) = 0 \ , \tag{3-1}$$

can be obtained. However, because of the randomness of the refractive index, n(x), along the path of propagation, an exact solution is very difficult. Approximation methods, notably Rytov's [30], have been used to solve the equation. He assumes that the general solution can be written as a sum of small perturbation terms, with the object wave being expressed as

$$E(x) = e^{\psi(x)} \ , \tag{3-2}$$

where

$$\psi = \psi_0 + \psi_1 \ ; \tag{3-3}$$

ψ_o is the solution in the absence of turbulence and ψ_1 is the first perturbation term. ψ is a function of the phase (θ) and amplitude (A) of the object wave, i.e.,

$$\psi_o(x) = \ln A_o(x) + i\theta_o(x) \ , \tag{3-4a}$$

$$\psi_1(x) = \ln \frac{A(x)}{A_o(x)} + i[\theta(x) - \theta_o(x)] \ . \tag{3-4b}$$

To simplify the form of the perturbative solution, ψ_1, two terms will be defined: the log-amplitude, χ, and the phase, S, of the wave, where

$$\chi \triangleq \ln A/A_o \ , \tag{3-5a}$$

$$S \triangleq \theta - \theta_o \ . \tag{3-5b}$$

Since these two functions are dependent on a statistically fluctuating parameter, the refractive index, they too will be statistical in nature. After characterizing the turbulence of the medium an analysis of these two functions will be presented.

Turbulence Statistics

At the end of Chapter I it was pointed out that the fluctuations in the temperature and pressure in a medium induced refractive index changes within that medium. Turbulence is then the local refractive index change (density gradient) of the medium. For homogeneous and isotropic turbulence a theory developed by Kolgomorov [18] can be used to characterize the statistical deviations in the refractive index induced by density gradients. Kolgomorov uses a quantity called the structure function, D_f, to determine the

fluctuations of a parameter f at two different points, x and x'. This function is defined as

$$D_f = \langle [f(x) - f(x')]^2 \rangle \ , \tag{3-6}$$

where < > denotes the ensemble average. If the difference of f at the two points, x and x', is determined mainly by inhomogeneities of sizes $|x - x'|$, then in the case where $|x - x'| \ll L_o$ (L_o is called the outer scale of turbulence), the quantity $f(x) - f(x')$ can be considered locally isotropic. For the range of values $\ell_o \ll |x - x'| \ll L_o$ (where ℓ_o is the inner scale of turbulence), the structure function depends on $r = |x - x'|$ and can be expressed by the "two-thirds" law, i.e.,

$$D_f = C_f^2 \, r^{2/3} \ , \tag{3-7}$$

where r is the correlation distance between the two observation points which are normal to the beam propagation path; C_f is called the structure constant, and is a constant, independent of r, which varies in magnitude by as much as three or four orders, depending on the strength of turbulence.

Assuming the refractive index, n, and the temperature, T, of the medium follow Kolgomorov's theory, structure functions can then be defined for each, i.e.,

$$D_n = C_n^2 \, r^{2/3} \ , \tag{3-8a}$$

$$D_T = C_T^2 \, r^{2/3} \ . \tag{3-8b}$$

In the atmosphere the turbulence due to relative temperature fluctuations is much stronger than the relative pressure fluctuations, so that the refractive index variations may be related to temperature variations. Hufnagel and Stanley [27] have derived the following relation between the two structure functions:

$$D_n = [\, 10^{-6} \; \rho/\rho_o \,]^2 \; D_T \; . \tag{3-9}$$

By using Eqs. (3-8a, 3-8b) in Eq. (3-9) a relationship between structure constants is obtained, i.e.,

$$C_n^2 = [\, 10^{-6} \; \rho/\rho_o \,]^2 \; C_T^2 \; , \tag{3-10}$$

where ρ/ρ_o is the relative density of the air at a specific pressure and temperature.

Therefore, the temperature structure function and constant can be determined by using high frequency response probes to measure the temperature at two points along the beam path. Then, by using the relationship between the refractive index and temperature (Eq. (3-10)), one can determine the refractive structure constant, a measure of the strength of turbulence.

Phase Degradation

Once the refractive index structure constant, C_n^2, has been established as a measure of the strength of turbulence, then the statistical fluctuations of the phase and log-amplitude of a wave propagating through a random medium must be analyzed. In this section the analysis will differentiate between spherical and planar waves.

Optically and holographically this is important in that spherical waves are representative of the diffracted waves from point objects, while planar waves represent the object illuminator and the field background.

The phase degradation of a propagating wave in a turbulent medium is such that the phase [26] is advanced or retarded a given number of wavelengths, giving rise to a distortion of the shape of the wavefront (i.e., loss of spatial coherence). The phase distribution across the spherical wavefront received by an optical system determines the complex optical transfer function of the image. The system's optical transfer function is the normalized Fourier transform of the light intensity distribution of a point object in the image plane.

Hufnagel and Stanley [27] have shown that the total modulation transfer function (MTF), the modulus of the optical transfer function, can be broken down into a product of two MTF's; one for the medium and one for the lens system, i.e.,

$$M_{total} = M_{medium} \cdot M_{lens} \ . \tag{3-11}$$

This is graphically represented in Fig. 3-1 [31]. As can be seen, the total MTF can be dominated by the medium. For short exposure the average MTF of the medium has been shown [27] to be

$$\langle M \rangle_{medium} = \exp[-D_s(r)] \ , \tag{3-12}$$

where $D_s(r)$ is the phase structure function, defined by Eq. (3-6). The phase structure function is a measure of the spatial coherence between two points, separated by a distance r, along the beam wavefront. If the beam is spatially coherent, $D_s(r)$ is zero and the total MTF of the

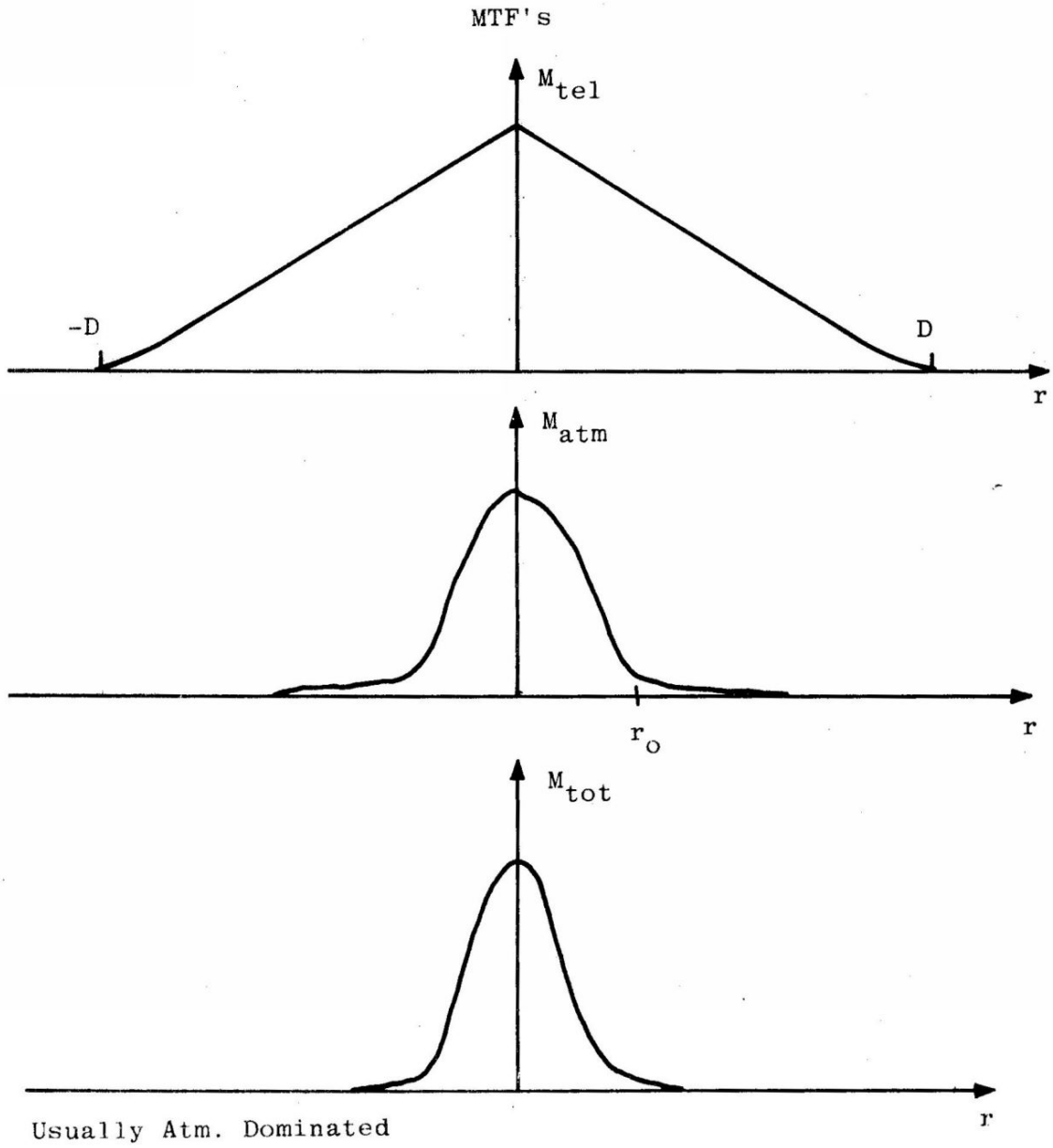

Figure 3-1. Modulation transfer function (MTF) of total optical system [31].

system is just that of the lens. Tatarski has related the phase structure function to the strength of turbulence, the propagation path, and the wavenumber, k, of the radiation by

$$D_s(r) = 2.91\ k^2 L C_n^2\ r^{5/3}\ . \tag{3-13}$$

Fried has simplified the form of the phase structure function by introducing a quantity r_o, called Fried's coherence length, to characterize the strength of turbulence, the propagation length, and the wavenumber, i.e.,

$$(1/r_o)^{5/3} \propto k^2 L C_n^2\ . \tag{3-14}$$

Using the above relation, Eq. (3-13) can be rewritten as

$$D_s(r) = 6.88(r/r_o)^{5/3}\ . \tag{3-15}$$

Using the MTF, Fried [19] has shown that the medium acts in such a way as to degrade the resolution capability of the optical system. Quantitatively, "Fried's resolution" is defined as the *integral over spatial frequencies, f, of the system's MTF, i.e.,*

$$\mathcal{R} = \int M(f)df\ . \tag{3-16}$$

A plot of the normalized resolution for short exposure versus normalized collecting aperture is given in Fig. 3-2. The interpretation of the graph is as follows:

1. For a given collecting aperture diameter, D, and for low turbulence the resolution is asymptotic to line 1, which is

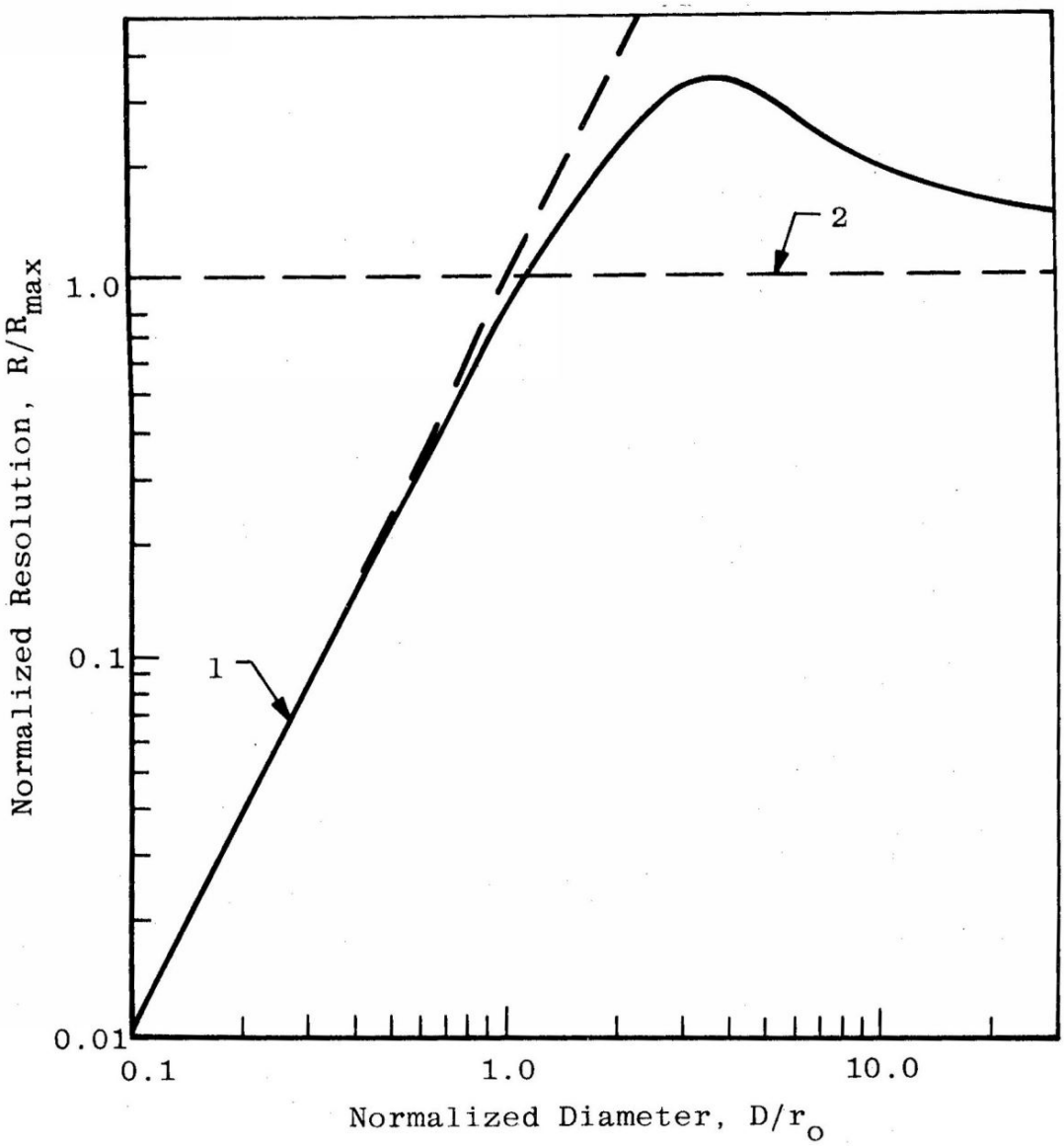

Figure 3-2. Normalized resolution for short exposure [26].

the aperture limiting resolution of the imaging optical system.

2. As the turbulence increases, the resolution approaches a constant, line 2, given by [20]

$$R_{max} = (\frac{\pi}{4})(\frac{r_o}{\lambda Z}) \ , \tag{3-17}$$

which is a measure of the finest detail that it is possible to see through a turbulent medium at a distance Z. The minimal resolvable length, δ, is given by

$$\delta = (4\ R_{max})^{-1/2} \ . \tag{3-18a}$$

Substituting Eq. (3-17) into Eq. (3-18a) yields

$$\delta = \pi^{-1/2}\ Z\ \frac{\lambda}{r_o} \ , \tag{3-18b}$$

which defines the resolution achievable by a diffraction limited "lens" of diameter r_o, where r_o is Fried's coherence length, defined by Eq. (3-14).

3. For a given set of turbulence conditions, characterized by $1/r_o$, the resolution peaks with increasing aperture size when D is on the order of 3.5 r_o. Past this point the resolution is turbulence limited, which is well below the diffraction limited resolution. Therefore, increasing the aperture of the imaging system beyond 3.5 r_o adversely affects the system's resolution.

The observed effect of object rays refracting from their original path is the spreading of the reconstructed image size and/or the inability to bring a particle into focus. Focusing a particle depends on the image contrast and edge sharpness. Because of angular deviations, rays will converge in different planes, reducing the image brightness and edge sharpness; thereby making particle size measurements difficult, if not impossible. The average angular spread [32], $\langle\phi\rangle$, is found to be proportional to the degree of turbulence and the distance, L, the object is from the recording medium, i.e.,

$$\langle\phi\rangle \propto C_n^2 L \quad . \tag{3-19}$$

While the structure function was used to measure the phase differences along the beam wavefront, the degree of fluctuation of the log-amplitude will be measured by a quantity called the variance. Statistically, the variance of a parameter f is defined [18] as

$$\sigma_f^2 \triangleq \langle [f(x) - \langle f(x)\rangle]^2 \rangle \quad , \tag{3-20}$$

where $\langle\ \rangle$ represents time averaging. The variance of the log-amplitude [21] is related to the strength of turbulence, C_n^2, the propagation length, L, and the wavenumber, k, of the radiation by

$$\sigma_\chi^2 \propto k^{7/6}\, L^{11/6}\, C_n^2 \quad . \tag{3-21}$$

The left-hand side of Eq. (3-21) can be written explicitly as

$$\sigma_\chi^2 = \langle [\ell n\ A/A_o]^2 \rangle \quad . \tag{3-22}$$

Since the intensity is expressible in terms of the wave amplitude, i.e.,

$$I = |A|^2 , \tag{3-23}$$

the log-amplitude variance can be related [18] to an experimentally measurable quantity, the intensity variance, by

$$\sigma_I^2 \triangleq < [\ell n\ I/I_o]^2 > = 4\sigma_\chi^2 . \tag{3-24}$$

From Eqs. (3-21, 3-24) it is obvious that as the turbulence level increases so does the amplitude of intensity fluctuation across the beam wavefront.

If the number density within the object scene is low then most of the light reaching the film will be planar. The observed intensity distribution on the film will then obey Eq. (3-24); that is, it will be mottled by the turbulence. When no turbulence is present the film will be evenly illuminated. As the level of turbulence increases, the density gradients along the path of propagation refract the light rays from their original path, causing areas of the film to be more illuminated than others. Since the intensity variance is inversely proportional to the wavelength ($k = 2\pi/\lambda$) of the radiation, the refractive index changes can be thought of as small prisms along the propagation path that refract the light. This is illustrated in Fig. 3-3. The longer the wavelength, the less refractive effects observed.

The breaking up of the uniformity of the beam intensity is observed in the reconstruction of a hologram. The reconstructed image is superimposed on a background, which idealistically is sought to be

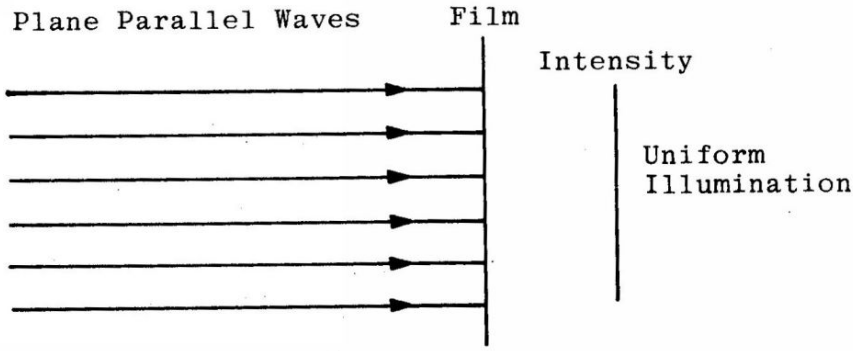

a) No turbulence in path of propagation
Result: Uniform film illumination

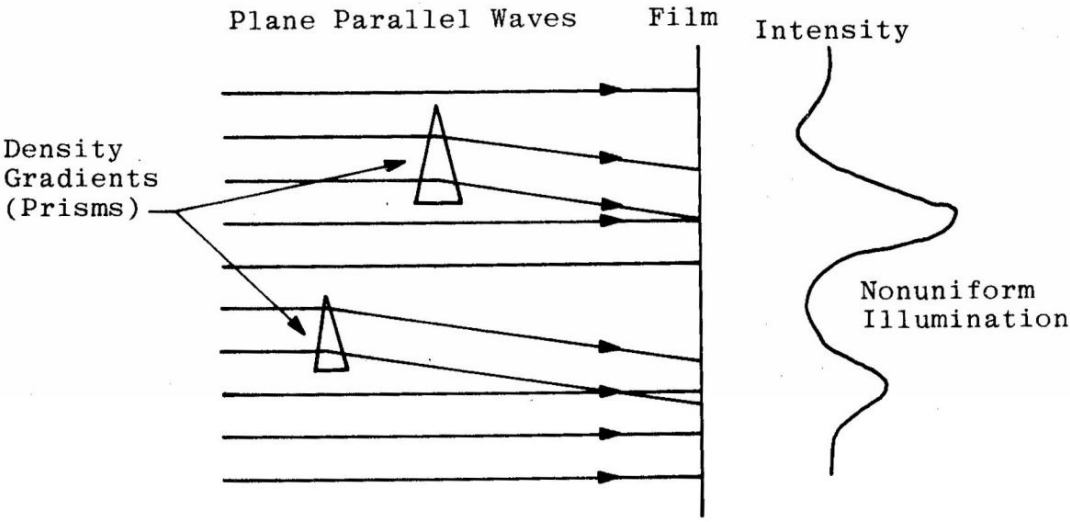

b) Turbulence (density gradients) act as prisms to refract light
Result: Nonuniform film illumination

Figure 3-3. Turbulence effect on intensity distribution.

a uniform field. However, turbulence can cause this background to be mottled to such a degree that it is sometimes difficult to identify particular images. The ability to discern the particles from the background depends on the size and intensity of the mottling. If the size of the blotches is comparable to the size of the particles, recognition of particulates may be impossible. This may result in some of the background being counted as particles, especially near the resolution limit of the optical system; resulting in a particle count uncertainty within that size region.

Mottling of the background by turbulence is a constant, dependent on the strength of turbulence and the length of beam propagation through media; whereas, the degree of image degradation is dependent on its position within the medium; that is, images of particles near the receiving optics will be less distorted than those near the laser. On the other hand, because turbulence reduces the spatial coherence of the light beam, the reconstructed particle images close to the receiving optics will be illuminated with pseudo-diffuse light, reducing (or eliminating) the particle's diffraction rings [33, 34]. Without these rings, image recognition against the mottled background is difficult.

CHAPTER IV

DISCUSSION

Within Chapter III the analysis of the effects of turbulence on a side-band holography system has been reduced to an analysis of the amplitude and phase variations of plane and spherical waves propagating through a randomly varying medium. The results have then been applied to the holographic system. To summarize, the effects of turbulence (defined as random refractive index changes of the medium along the path of beam propagation) on the holographically reconstructed object field are a mottling of the background and a loss of image resolution.

In addition to the effects of turbulence on the holographic images, methods to determine the levels of turbulence (in terms of the refractive index structure constant), the beam intensity fluctuations (in terms of log-amplitude variance), and the phase degradation along the wavefront (in terms of the phase structure function) have been presented in terms of the medium measurables, the pressure and temperature fluctuations. A relationship between the wind tunnel parameters and holographic image quality will be made within this chapter.

Within the APTU air mixer, random refractive index variations, caused by local density inhomogeneities, were measured as pressure fluctuations. Since atmospheric analysis of turbulence effects on beam propagation is based on random refractive index variations, the analysis is also valid for the conditions within the APTU wind tunnel.

A first-order calculation can be made to determine the amount of phase change that is induced by a turbulence on the wavefront of a

propagating laser beam. The phase difference of a ray propagating in a medium, characterized by randomly varying refractive indices, will be considered. From Chapter I the phase difference between two rays passing through a turbulent medium was expressed as:

$$\Delta\theta \approx \frac{2\pi}{\lambda} L(n-1) \left(\frac{\Delta P}{P} - \frac{\Delta T}{T}\right) , \qquad (1\text{-}14)$$

where ΔP and ΔT are differences in pressure and temperature. From the APTU conditions, i.e., light beam propagation length through the mixer of 2.1 meters, hologram recording wavelength of 0.6943 μm, refractive index of 1.000275, and using the ΔP_{RMS} relative pressure fluctuation from Fig. 2-3, page 14, as 0.7%, a phase change of 11.6π is obtained. This indicates that the air stream within the wind tunnel is capable of inducing phase changes. This calculation ignored temperature fluctuations for reasons stated previously. With no airflow within the test cell, $\Delta P = 0$, and no phase change is expected. However, with airflow on, $\frac{\Delta P}{P} \approx 0.7\%$, and a 11.6π phase change is induced for the images formed near the far port window, i.e., L = 2.1 meters. Comparing the far reticle images formed under these two conditions, an increase in image resolution from 120 to 450 meters is observed. For particles near the far port window the 11.6π phase change was so large that no particle data were obtained. However, for particles near the receiving optics, where L = 1 meter, the phase change was small enough, 5.8π, to obtain particle image data.

Equation (1-14) indicates that an increase in test cell pressure yields a corresponding phase change. In Chapter III it was pointed out that phase changes in a planar beam induce intensity

variations across the beam cross section and should be holographically observed as background mottling. Holograms taken at the APTU air mixer, under various pressures, confirm this theory. From these holograms it was found that as the test cell pressure increased so did the background mottling. The size of the background "blotches" was found to be inversely proportional to cell pressure, Fig. 2-12, page 29, indicating a higher degree of intensity variances across the photographic film. The ability to discern particles from background depended on the size and intensity of the mottling. When the size of the blotches approached the size of the particle images recognition of particles became difficult, resulting in some of the background noise being counted as particles. Because of this, holograms recorded above 60 psia yielded no reliable particle image data.

A graph, based on Eq. (1-14), of phase change as a function of P/T is used to demonstrate holographic quality, for two given propagation lengths. Figure 4-1 shows the limits of good, marginal, and bad quality based on reconstructed holograms of given pressures and temperatures. It should be noted that phase change is inversely proportional to temperature, indicating that better holograms should be recorded at higher temperatures. A more detailed study of holographic imagery as a function of turbulence is needed to define the range of expected image quality. Once this is done, one can predict the degradation effects and expected image quality based on a given set of medium conditions.

A better analysis of the phase changes induced by refractive index inhomogeneities can be obtained from the phase structure function,

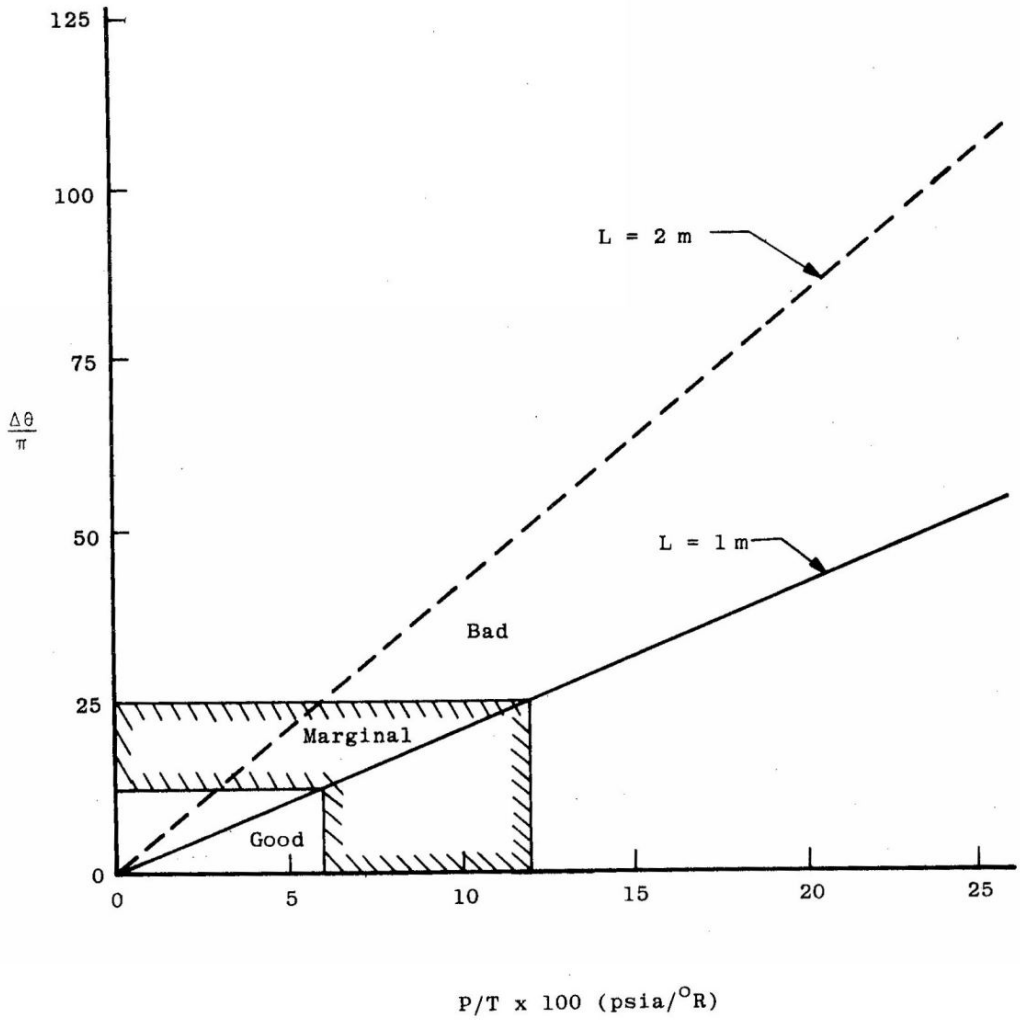

Figure 4-1. Hologram quality as a function of phase change.

D_s, expressed by Eq. (3-13), i.e.,

$$D_s = 2.91\ k^2 L C_n^2\ r^{5/3}\ , \qquad (3\text{-}13)$$

where C_n^2 is the refractive index structure constant, a measure of the the turbulence along the beam propagation path. The problem in applying this equation to the test conditions at APTU is that C_n^2 is unattainable from pressure data recorded during the test, since the pressure fluctuations were averaged over time and no cross-correlation between probes on the control rake was made.

The method of obtaining C_n^2 data is complex and offers an opportunity for future investigation. Three possible methods will be described that can be used in obtaining C_n^2. The most direct measurement method uses high-frequency temperature and pressure probes, as was described in Chapter III. To determine the structure function, three conditions must be satisfied: 1) the turbulence must be homogeneous and isotropic, 2) the correlation distance, r, must be such that $\ell_o << r << L_o$, where ℓ_o and L_o are the inner and outer scales of turbulence [18], and 3) the probes must have a frequency response high enough to measure the smallest fluctuations of the measured parameter. In APTU, the first condition is satisfied since the total pressure distortion profile (Fig. 2-4, page 16) was almost uniform across the air mixer, indicating homogeneity of turbulence. The outer scale of turbulence can be assumed to be the size of the air mixer, while the inner scale, the size of the smallest inhomogeneities that can exist in the airflow, can be calculated from the Reynolds number of the airflow by [18]: $\ell_o \sim L_o/Re^{3/4}$. The Reynolds number in APTU ranged from 400 to

14,000, depending on operating conditions, and yielded scales of inner turbulence between 1.6 mm and 2.3 cm. This value is consistent with the one obtained by considering the size of the mesh screen (Fig. 2-2, page 12) that was installed to reduce the scale of the turbulent eddies. The screen is a 6 x 6 mesh, indicating eddy sizes on the order of 0.3 cm.

The third criterion to be satisfied is the frequency response range of the instruments. From the above maximum and minimum values of eddy sizes and assuming typical air velocities to be 10 m/sec, a frequency response range of 5 to 2000 Hz should be expected. Although the APTU instrumentation response ranged from 5 to 2000 Hz, with a 2-db attenuation of the signal in the range 500 to 2000 Hz, no data were available above 500 Hz. However, in the 5 to 500 Hz range, $\Delta P_{RMS}/P_{total}$ was 0.7%. Since the wind tunnel conditions satisfy the structure function criteria, the value of C_n^2 calculated from probe measurements of pressure and temperature could be used to characterize the strength of the turbulence within the air mixer.

In Chapter II it was established that intensity fluctuations across a beam wavefront are caused by turbulence and are related by Eq. (3-24). Therefore, by measuring the variance of the intensity fluctuations the strength of turbulence, C_n^2, can be calculated. The intensity fluctuations of a laser beam propagating across a turbulent medium are measured with a fast-response photodetector. The detector must be fast enough to measure changes caused by the smallest of the inhomogeneities. As the turbulence increases so (theoretically) does the intensity variance. Experimental evidence has shown, however, that saturation [35, 36] occurs when the variance reaches 0.5. Little is

known about the cause of saturation, except that it occurs for optical wavelengths or shorter, at long distances, and for strong turbulent conditions. Since Rytov's approximation is not able to account for saturation, a modified theory [36] to include higher order scattering has been developed and shown to fit experimental curves. The expression for the intensity variance, σ_I^2, is given by

$$\sigma_I^2 = \ln [2 - \exp (- 4 \sigma_\chi^2)] , \qquad (4\text{-}1)$$

where σ_χ^2 is the log-amplitude variance defined by Eq. (3-22). At low turbulence conditions, Eq. (4-3) approaches Eq. (3-24). An estimate of the strength of turbulence, C_n^2, inside the APTU wind tunnel corresponding to saturation of the intensity variance can be made using Eq. (3-24), i.e.,

$$C_n^2 = \frac{\sigma_I^2}{1.2\ k^{7/6}\ L^{11/6}} . \qquad (3\text{-}24)$$

To be the case in APTU, C_n^2 would have to be on the order of $10^{-9}\ m^{-2/3}$. This value, compared to those obtained in the atmosphere, corresponds to very strong turbulence. In the atmosphere saturation can occur at lower values of C_n^2 since the propagation distance is much longer (100 to 2000 meters) than through the APTU air mixer (i.e., 2 meters). At present, no value of σ_I^2 has been calculated for the Arnold Center wind tunnel facility.

An alternative method of measuring the refractive index structure constant is available by using the holograms which were recorded at the APTU mixer air stream. Since a hologram records all of

the information about the medium through which the object beam propagates the reconstructed volume image, or the hologram itself can be scanned with a small area photodetector to obtain the variance of the intensity fluctuations. Since it has been shown that the turbulence induces intensity variations across the film plane, these spatial variations should be related, by Taylor's hypothesis, to the temporal variations as measured by σ_I^2.

At the conclusion of this study it became apparent that there was not enough time to obtain these data points. It is recommended that this experiment be performed so the strength of turbulence, measured as C_n^2, can be determined for the various conditions under which the holograms were recorded. The calculated values of the structure constant can then be correlated to image quality and to determine if saturation occurred.

CHAPTER V

SUMMARY, CONCLUSIONS, AND RECOMMENDATIONS

The objective of this work was two-fold. First, to demonstrate the conditions under which side-band holograms could be taken in a high temperature/pressure environment for reliable particle size data. Second, to analyze the effects of turbulence on the side-band holographic particle sizing technique. As to the first objective, holograms were taken at various combinations of test cell pressure and temperature and data reduced for particle size. The effects of increasing turbulence were observed and documented: background mottling, loss of spatial coherence, and loss of image resolution. A literature survey of laser beam propagation through a randomly varying medium served to explain the observed effects in terms of amplitude and phase changes of planar and spherical waves. The result of this analysis is that the observed effects are directly proportional to the strength of air turbulence and the length of propagation, but inversely proportional to the wavelength of the radiation.

The obvious conclusion from this is that in order to reduce the turbulence effects, and since nothing can be done about the strength of turbulence, the distance that the beam must traverse the medium should be reduced. One method would be to protect the beam with cylindrical pipes installed in the test section. However, care should be taken such that the installation of these pipes does not alter the medium that is being observed.

Another solution is to use longer wavelengths in the recording process, since these are less affected by refractive index changes. However, for particle sizing shorter wavelengths are sought so that small particles (less than 10 microns in size) can be recorded. It appears then that the choice of wavelength must be a compromise between the size of the particles being investigated and the amount of turbulence degradation that can be tolerated.

Still another approach is to modify the optical system in the recording or reconstruction process to compensate for the turbulence effects. One example is the use of ground glass, placed in front of the laser in the recording process [5]. The ground glass scatters the light over wide angles averaging out the refractive effects. Diffuse light images, however, suffer from laser speckle effects, which can degrade the resolution by a factor of two over the coherent case. Particle sizing in the region of speckle has been facilitated by use of a rotating translucent screen [5] in the reconstruction process. The screen suppresses speckle noise, resulting in an apparent improvement of the resolution.

An alternative to in-line and side-band holography is Fourier-lensless holography. Gaskill [12] has gone through a mathematical analysis with both the reference and object beams propagating through turbulent media and has shown that for short exposure imagery the field of view is not limited by the perturbative medium, but the region of high resolution is limited. Within this region, which is centered at the reference position, the intensity distribution consists of nearly diffraction limited images superimposed on a noiselike background, the strength of which depends on the turbulence. On the average, however,

this undesired background vanishes for r, the distance of the object to the reference point, greater than $1.8(\lambda Z)^{1/2}$ and will affect only the images which are less than r. Past this point the resolution is two-thirds that of conventional imagery without the presence of turbulence.

The problem of applying Fourier-lensless holography to particle field analysis is that the reference beam must be focused in one plane of the flow field. This being the case, only the region around the focal plane can be used for analysis, thereby eliminating the longitudinal scanning capability inherent to in-line and side-band holography.

An important facet of the holographic process is the requisition of particle data from the reconstructed volume. Normally, data reduction is done by a trained observer who can visually recognize an image, bring it into focus and then measure its size. The work is both tedious and time consuming. New image analysis systems are now available that can automatically scan the reconstructed volume, search out particles, bring them into focus, and measure their size, shape, and position; all under the control of a computer. This method removes all subjectivity in the reconstruction process and human judgment errors from the particle data. However, this system works best [37] only under ideal conditions, i.e., no (or only minimal) background mottling can be tolerated. Extension to poor signal-to-noise images lies in the development of algorithms that can be used in bringing a particle into focus or distinguishing a particle from the mottled background. An understanding of turbulence effects on holography will be helpful in achieving the final goal of automation.

BIBLIOGRAPHY

BIBLIOGRAPHY

1. Goodman, J. W. Introduction to Fourier Optics. New York: McGraw Hill Book Company, 1968.

2. Smith, H. M. Principles of Holography. New York: John Wiley and Sons Book Company, 1975.

3. Hunt, J. D. "Engine Icing Measurement Capabilities at the AEDC." Paper presented at the AGARD Propulsion and Energetics Panel Fifty-First Specialists Meeting, London, England, 1978.

4. Lennert, A. E., et al. "Electro-Optical Techniques for Diesel Engine Research." AIAA Paper No. 76-68, presented at AIAA Aerospace Sciences Meeting, Washington, D. C., January, 1976.

5. Briones, R. A., and R. W. Wuerker. "Holography of Solid Propellant Combustion," Society of Photo-Optical Instrumentation Engineers, 125:90-95, August, 1977.

6. Belz, R. A., and N. S. Dougherty. "In-Line Holography of Reacting Liquid Sprays," Proceedings of the Engineering Application of Holography Symposium. Los Angeles: Society of Photo-Optical Instrumentation Engineers, 1972. Pp. 209-218.

7. Wolfe, W. L. (editor). Handbook of Military Infrared Technology. Washington, D. C.: Office of Naval Research, Department of the Navy, 1965.

8. Hodgemon, C. D. (editor). Handbook of Chemistry and Physics. Forty-fourth edition. Cleveland, Ohio: Chemical Rubber Publishing Company, 1963.

9. Carter, P. B., and W. A. Turrintine. "Investigation of Flow Dynamics in a Blowdown Type Propulsion Wind Tunnel." AIAA Paper No. 77-990, presented at AIAA Thirteenth Propulsion Conference, Orlando, Florida, July, 1977.

10. Thompson, B. J., J. H. Ward, and W. R. Zinky. "Applications of Hologram Techniques for Particle Size Analysis," Applied Optics, 6:519-526, March, 1967.

11. Menzel, R. W. "Fundamental Properties of Holographic Reconstructed Images." Unpublished Master's thesis, The University of Tennessee, Knoxville, 1975.

12. Gaskill, J. D. "Imaging through a Randomly Inhomogeneous Medium by Wavefront Reconstruction," Journal of Optical Society of America, 58:600-608, May, 1968.

13. Gaskill, J. D. "Atmospheric Degradation of Holographic Images," Journal of Optical Society of America, 59:308-318, March, 1969.

14. Leith, E. N., and J. Upatnicks. "Holographic Imagery through Diffusing Media," Journal of Optical Society of America, 56:523, April, 1966.

15. Goodman, J. W., W. H. Huntley, Jr., et al. "Wavefront-Reconstruction Imaging through Random Media," Applied Physics Letters, 8:311-313, June, 1966.

16. Bryngdahl, Olaf. "Holographic Penetration of an Inhomogeneous Medium," Journal of Optical Society of America, 59:1245-1246, September, 1969.

17. Stetson, K. A. "Holographic Fog Penetration," Journal of Optical Society of America, 57:1060-1061, August, 1967.

18. Tatarski, V. I. Wave Propagation in a Turbulent Media. Translated from the Russian by R. A. Silverman. New York: McGraw Hill Book Company, 1961.

19. Fried, D. L. "Optical Resolution through a Randomly Inhomogeneous Medium for Very Long and Very Short Exposures," Journal of Optical Society of America, 56:1372-1379, October, 1966.

20. Fried, D. L. "Limiting Resolution Looking Down through the Atmosphere," Journal of Optical Society of America, 56:1380-1384, October, 1966.

21. Fried, D. L., and J. D. Cloud. "Propagation of an Infinite Plane Wave in a Randomly Inhomogeneous Medium," Journal of Optical Society of America, 56:1667-1676, December, 1966.

22. Fried, D. L. "Optical Heterodyne Detection of an Atmospherically Distorted Signal Wave Front," Proceedings of the IEEE, 55:56-67, January, 1967.

23. Fried, D. L. "Propagation of a Spherical Wave in a Turbulent Medium," Journal of Optical Society of America, 57:175-180, February, 1967.

24. Fried, D. L., and J. B. Seidman. "Laser Beam Scintillation in the Atmosphere," Journal of Optical Society of America, 57:181-185, February, 1967.

25. Fried, D. L. "Propagation of the Mutual Coherence Function for an Infinite Plane Wave through a Turbid Medium," Optics Letters, 1:104-106, September, 1977.

26. Fried, D. L. "Advanced Imaging Techniques: Concept and Understanding," Society of Photo-Optical Instrumentation Engineers, 125:6-21, August, 1977.

27. Hufnagel, R. E., and N. R. Stanley. "Modulation Transfer Function Associated with Image Transmission through Turbulent Media," Journal of Optical Society of America, 54:52-61, January, 1964.

28. Villars, F., and V. F. Weisskopf. "The Scattering of Electromagnetic Waves by Turbulent Atmospheric Fluctuations," Physical Review, 94:232-240, April, 1954.

29. Reynolds, G. O., and T. J. Skinner. "Mutual Coherence Function Applied to Imaging through a Random Medium," Journal of Optical Society of America, 54:1302-1309, November, 1964.

30. Ho, T. L. "Log-Amplitude Fluctuations of Laser Beam in a Turbulent Atmosphere," Journal of Optical Society of America, 59:385-390, April, 1969.

31. Greenwood, D. "Propagation in a Turbulent Atmosphere." Paper presented at a short course entitled "Aspects of Atmospheric Optics," The University of Tennessee Space Institute, Tullahoma, Tennessee, May, 1977.

32. Coulman, C. E. "Dependence of Image Quality on Horizontal Range in a Turbulent Atmosphere," Journal of Optical Society of America, 56:1232-1238, October, 1966.

33. Lurié, M. "Effects of Partial Coherence on Holography with Diffuse Illumination," Journal of Optical Society of America, 56:1369-1372, October, 1966.

34. Considine, P. S. "Effects of Coherence on Imagine Systems," Journal of Optical Society of America, 56:1001-1008, August, 1966.

35. Strohbehn, J. W. "Line-of-Sight Wave Propagation through the Turbulent Atmosphere," Proceedings of the IEEE, 56:1301-1318, August, 1968.

36. deWolf, D. A. "Saturation of Irradiance Fluctuations due to Turbulent Atmosphere," Journal of Optical Society of America, 58:461-466, April, 1968.

37. Jones, A. R., M. Sarjeant, et al. "Application of an In-Line Holography to Drop Size Measurements in Dense Fuel Sprays." Letter to the Editor, Applied Optics, 7(No. 3):328-330, February, 1978.

VITA

Stanley Z. Peplinski was born on July 14, 1953, in Lesko, Poland. He immigrated to the United States in 1961 and six years later became a naturalized citizen.

He attended parochial schools in Chicago, Illinois, graduating as a Salutatorian from Holy Trinity High School. In May, 1976, he graduated from The Illinois Institute of Technology with a Bachelor of Science degree in Physics. In October, 1976, he entered The University of Tennessee Space Institute in Tullahoma, Tennessee, on a Graduate Research Assistantship and began study towards a Master's degree in Physics. He performed his research at the Advanced Concepts Staff of Arnold Engineering Development Center.

After receiving his degree in June, 1978, he moved to Albuquerque, New Mexico, where he began full-time employment for the Dynalectron Corporation.